

Interannual Variability of the Natal Pulse

Yoko Yamagami¹, Tomoki Tozuka², and Bo Qiu³**Key Points:**

- Interannual variations of the Natal Pulse are explained by the number of anticyclonic eddies arriving at the Natal Bight
- Southeast Madagascar Current is the main source of eddies which propagate to the Natal Bight, and thus the main source of the Natal Pulse
- Significant relationship between interannual variations of the Natal Pulse and wind stress curl field in the southern Indian Ocean is found

Correspondence to:Y. Yamagami,
yamagami@aori.u-tokyo.ac.jp**Citation:**Yamagami, Y., Tozuka, T., & Qiu, B. (2019). Interannual Variability of the Natal Pulse. *Journal of Geophysical Research: Oceans*, 124, 9258–9276. <https://doi.org/10.1029/2019JC015525>

Received 26 JUL 2019

Accepted 19 NOV 2019

Accepted article online 4 DEC 2019

Published online 17 DEC 2019

¹Atmosphere and Ocean Research Institute, The University of Tokyo, Kashiwa, Chiba, Japan, ²Department of Earth and Planetary Science, Graduate School of Science, The University of Tokyo, Tokyo, Japan, ³Department of Oceanography, University of Hawaii at Manoa, Honolulu, Hawaii, USA

Abstract Satellite altimetry data and high-resolution model output are used to investigate the mechanism of interannual variations of the solitary meander in the Agulhas Current, called the Natal Pulse. It is shown that most of the Natal Pulses are triggered by anticyclonic eddies originating from the Southeast Madagascar Current (SEMC) and anticyclonic eddies of the Mozambique Channel are the secondary source. In addition to the barotropic conversion suggested by previous studies, the advection of eddy kinetic energy (EKE) plays a statistically significant role in the growth of the Natal Pulse. The number of anticyclonic eddies arriving at the Natal Bight largely explains the interannual variations in the Natal Pulse. The barotropic conversion from the SEMC, whose interannual variations are likely related to the remote wind forcing, is the main EKE source and corresponds well with the interannual variations of anticyclonic eddies generated off the southern coast of Madagascar. It is also shown that the interannual variations of the Natal Pulse are linked to large-scale wind variability in the southern Indian Ocean.

Plain Language Summary Natal Pulse is the large meander of the Agulhas Current originating in the Natal Bight and it affects both the local marine environment and global ocean circulation.

Previous observational studies suggested that the occurrence of the Natal Pulse varies from year-to-year. Since oceanic eddies tend to trigger the Natal Pulse, we investigate the relationship between the Natal Pulse and incoming eddies in this study. We show that variations of the Natal Pulse are mainly explained by variations of eddies propagating from the south of Madagascar and the Mozambique Channel. We also show that variations in the Natal Pulse are linked to the large-scale wind variability over the southern Indian Ocean. This study is the first to show the mechanism of the year-to-year variations in the Natal Pulse.

1. Introduction

The Agulhas Current is one of the strongest western boundary currents in the world oceans, transporting a tremendous amount of water mass and heat poleward along the South African coast. Its water mainly originates from mesoscale eddies from the Mozambique Channel (MC), and the Northeast and Southeast Madagascar Currents (NEMC and SEMC). Further upstream, almost half of the water in the NEMC and SEMC is fed by water masses from the South Equatorial Current, while the other half comes from south of Australia as a branch of the wind-driven subtropical gyre in the intermediate layer (Durgadoo et al., 2017). Because of its unique characteristics, the Agulhas Current attracted many oceanographers in recent decades (Beal et al., 2011; Beal et al., 2015; Beal & Elipot, 2016; Lutjeharms, 2006).

Understanding the role of the Agulhas Current in the inter-basin water mass exchange between the Indian and Atlantic Oceans has been a great motivation for in-situ and satellite altimeter observations as well as eddy-resolving numerical simulations. This is because the southwestern Indian Ocean is one of the most eddy-rich oceans owing to the presence of Madagascar (Penven et al., 2006), and mesoscale eddy variability in the Agulhas Retroflexion region seems to play a critical role in the global thermohaline circulation (Beal et al., 2011). This water mass exchange is known as the Agulhas Leakage, and influences the stratification of the upper branch of the Atlantic meridional overturning circulation and thus the long-term climate variations of the North Atlantic (Biastoch et al., 2008). Biastoch et al. (2015) reported that the Agulhas Leakage and Atlantic Multi-decadal Oscillation covary with the Agulhas Leakage leading by 15 years. Biastoch et al. (2009) attributed the recent increase in the Agulhas Leakage to the poleward shift of the westerly wind in the Southern Hemisphere associated with global warming. More recently, Durgadoo et al. (2013) and Loveday et al. (2014) conducted sensitivity experiments that highlight the relative contribution of changes in the westerly and trade wind to decadal variability of the Agulhas Leakage. They concluded that the

Agulhas Leakage predominantly responds to the strengthening of the westerly wind linearly and that the Agulhas Leakage is decoupled from the trade wind. On the other hand, the upstream control hypothesis also forms the foundation for research about the Agulhas Current and Leakage (Schouten et al., 2002). In their hypothesis, the meander of the Agulhas Current, the so-called “Natal Pulse” (Lutjeharms, 1981; Lutjeharms & Roberts, 1988) triggered by mesoscale eddies from the MC or south of Madagascar, leads to early retroflexion of the Agulhas Current and the ring shedding. The link between the Natal Pulse and the ring shedding is controversial since many Agulhas Rings are shed independently (Elipot & Beal, 2015), while some Natal Pulse events are linked to the early retroflexion occurrences (Krug & Tournadre, 2012).

Besides the importance of the Agulhas Current and its deflection on the global ocean circulation, the strong poleward transport of the Agulhas Current also has large impacts on the regional biodiversity around southern Africa. Strong surface currents in the Agulhas Current determine the distribution of marine animals such as Leatherback sea turtles (Hughes et al., 1998) and Jackass penguins (Randall et al., 1981). Also, the upwelling induced by topography in the vicinity of the Agulhas Current (Gill & Schumann, 1979) and wind forcing (Leber et al., 2016) feeds the ecosystem in the coastal region (e.g. Guastella & Roberts, 2016). The Natal Pulse also impacts on the biology of the Agulhas Current system. Water exchange between the coastal regions and the deep ocean associated with the Natal Pulse affects the biology of the Agulhas Bank (Krug et al., 2014). Therefore, the Natal Pulse is one of the key phenomena to understand physics and biogeochemistry in the Agulhas Current region.

The large deflection of the Agulhas Current was first detected by satellite infra-red images of sea surface temperature (SST) (Harris et al., 1978) and was later verified by hydrographic data off the east coast of southern Africa (Gründlingh, 1979). This meander received much attention not only because of its kinematics but also because it may lead to the early retroflexion of the Agulhas Current and pinching-off of the Agulhas Ring (Krug & Tournadre, 2012; van Leeuwen et al., 2000). Lutjeharms and Roberts (1988) analyzed over 9 years of satellite infra-red data and hydrographic data, and reported that the Natal Pulse usually propagates southwestward along the South African coast with the phase speed of around 20 km/day, although Rouault and Penven (2011) reported based on high-frequency SST imagery that most of the Natal Pulses generated in the Natal Bight do not reach the southern Agulhas Current region, but those that do not dissipate tend to grow downstream as reported in previous studies.

Many studies have investigated the generation mechanism of the Natal Pulse. de Ruijter et al. (1999) suggested that the strong meridional velocity over the local gentle topography in the Natal Bight is favorable for barotropic instability based on a linear stability analysis. More recently, however, Tsugawa and Hasumi (2010) conducted sensitivity experiments with a high-resolution ocean model to highlight the role of the local topography in the Natal Bight and showed that the topography is not necessary for the generation of the Natal Pulse. Rather, they concluded that anticyclonic eddies from the MC or south of Madagascar trigger the Natal Pulse through the barotropic conversion. In-situ observations support the idea that barotropic instability due to the horizontal shear of the Agulhas Current plays a major role in the formation of the Natal Pulse (Elipot & Beal, 2015). Also, several studies reported the periodicity and evolution of the Natal Pulse (Rouault & Penven, 2011), and the role of cyclonic eddies on the strength of meanders (Braby et al., 2016). Although many efforts have been devoted to modeling of the Agulhas Current, recent sophisticated ocean models still exaggerate eddy activities offshore of the Agulhas Current core (e.g. Backeberg et al., 2014; Durgadoo et al., 2013; Loveday et al., 2014; Siedler et al., 2009), and are unable to reproduce observed eddy dissipations (Braby et al., 2016).

There have been some debates over the frequency of Natal Pulse events. The frequency was estimated to be 4 to 6 per year from a moored current meter array from February 1995 to April 1996 (Bryden et al., 2005). On the other hand, Rouault and Penven (2011) analyzed an hourly SST product between June 2004 and October 2010 and reported that the frequency is 1.6 per year near the coast of Port Elizabeth (25°E, 34°S). As reported by Rouault and Penven (2011), inconsistency between these studies is due to the location where the Natal Pulse is defined. The differences in frequencies are also supported by other studies (Elipot & Beal, 2015; Krug et al., 2014; Krug & Tournadre, 2012). Krug and Tournadre (2012) examined the variability of the Natal Pulse from the satellite observation and they concluded that the Natal Pulse lacks seasonal variability.

Interannual variations of the Natal Pulse have been examined by many studies. Intermittent occurrences of Natal Pulses have been described (e.g. Lutjeharms et al., 2001; van Leeuwen et al., 2000), and Krug and

Tournadre (2012) reported an increase in the annual number of Natal Pulses detected near 34°S after 2001. Eliot and Beal (2015) investigated the time series of sea level anomaly (SLA) from October 1993 to August 2013 near the coast of East London (28°E, 33.6°S) and mooring observations, and found that the annual number of the Natal Pulse varied interannually from 0 to 4. Considering the importance of mesoscale eddies suggested by previous studies, interannual variations of the mesoscale eddies in this region may influence those of the Natal Pulse. However, the relationship between eddies and the Natal Pulse, especially on the interannual time scale, is not fully understood and this is a motive for this study.

In this study, we examine the details of interannual variations of the Natal Pulse events focusing on the roles of mesoscale eddies using satellite sea surface height (SSH) data and the high-resolution ocean general circulation model (OGCM) output. This paper is organized as follows. A brief description of the data, OGCM output, and eddy-tracking algorithm is given in the next section. In section 3, model validation is presented. Sources of the Natal Pulse are discussed in section 4. Interannual variability of the Natal Pulse and its possible mechanism are examined in section 5. The final section provides discussion and summary of this study.

2. Data and Methods

2.1. Data and Model

We use the altimeter-derived absolute dynamic topography (ADT) defined as the mean dynamic topography (MDT) plus sea level anomaly (SLA). The ADT products (DUACS DT2014; Pujol et al., 2016) are produced by Ssalto/Duacs and distributed by AVISO (are now produced and distributed by Copernicus Marine Environment Monitoring Service). We have analyzed daily data with a horizontal resolution of $1/4^\circ \times 1/4^\circ$. The period is from January 1993 to December 2015.

We have also analyzed output from the OGCM for the Earth Simulator (OFES) (Masumoto et al., 2004). The OFES is based on the version 3 of the Modular Ocean Model (MOM3) with optimization for the Earth Simulator. The computational domain is a semi-global region extending from 75°S to 75°N with a horizontal resolution of $0.1^\circ \times 0.1^\circ$ and 54 vertical levels. After the model is spun up for 50 years using the monthly mean forcing from 1950 to 1999 from the National Centers for Environmental Prediction (NCEP)/National Center for Atmospheric Research (NCAR) reanalysis data (Kalnay et al., 1996), a hindcast run from 1950 to 2013 was conducted using the daily NCEP/NCAR reanalysis data. In this study, 3-day snapshots after 1993 are analyzed for consistency with the AVISO ADT dataset. See Masumoto et al. (2004) for more details regarding the OFES hindcast.

2.2. Eddy-tracking method

To detect and track mesoscale eddies, we use the eddy-detection algorithm developed by Chelton et al. (2011). This detection technique is based on the geometry of closed SLA contours and it is as frequently used as methods that use the Okubo-Weiss parameter, wavelet transform, and Lagrangian coherent structures (e.g. Beron-Vera et al., 2013; Chelton et al., 2007; Halo, Backeberg, et al., 2014; Souza et al., 2011).

For the present analysis, “py-eddy-tracker” (Mason et al., 2014) is extended for the OFES output with slight changes in values of some parameters. In our analysis, we first apply a Gaussian filter with 50 km e-folding scale to SLA snapshots to reduce sub-grid scale errors and sampling biases. Also, SLA of the OFES is converted to the resolution of $0.25^\circ \times 0.25^\circ$ and interpolated into daily data. The other procedures are almost the same as those used by Mason et al. (2014). After a high-pass filter with wavelength scales of 20° in longitude by 10° in latitude is applied to the SLA fields to remove the basin-scale anomalies, all closed contours are tested. For the selection of an eddy, a closed contour must meet the following criteria:

1. Pass a shape test (Kurian et al., 2011) with an error smaller than 100%,
2. All SLA values are above (below) a given SLA threshold in anticyclonic (cyclonic) eddies,
3. More than 8 and fewer than 1000 pixels are inside of a given closed contour,
4. There is only one local SSH maximum (minimum) for anticyclonic (cyclonic) eddies, and
5. Amplitude is more than 1 cm and less than 150 cm.

Here, we set the criterion of shape test error to be 100%, trying to improve the traceability of mesoscale eddies.

The tracking method developed by Penven et al. (2005) is also used in py-eddy-tracker. In this method, if multiple eddies at the next time step are candidates for the same eddy, the eddy is classified using a dimensionless similarity parameter:

$$S = \sqrt{\left(\frac{\Delta d}{d_0}\right)^2 + \left(\frac{\Delta a}{a_0}\right)^2 + \left(\frac{\Delta A}{A_0}\right)^2} \quad (1)$$

Here, Δd is the separation distance, Δa is the area variation, and ΔA is the variation of amplitudes. Also, d_0 , a_0 , and A_0 are characteristic values for separation distance (25 km), area variation ($\pi 60^2 \text{ km}^2$), and variation of amplitude (2 cm), respectively. If S is minimum for a given eddy, this eddy is regarded as the same eddy at the next time step. Note that merging and splitting of eddies are not considered in this tracking method.

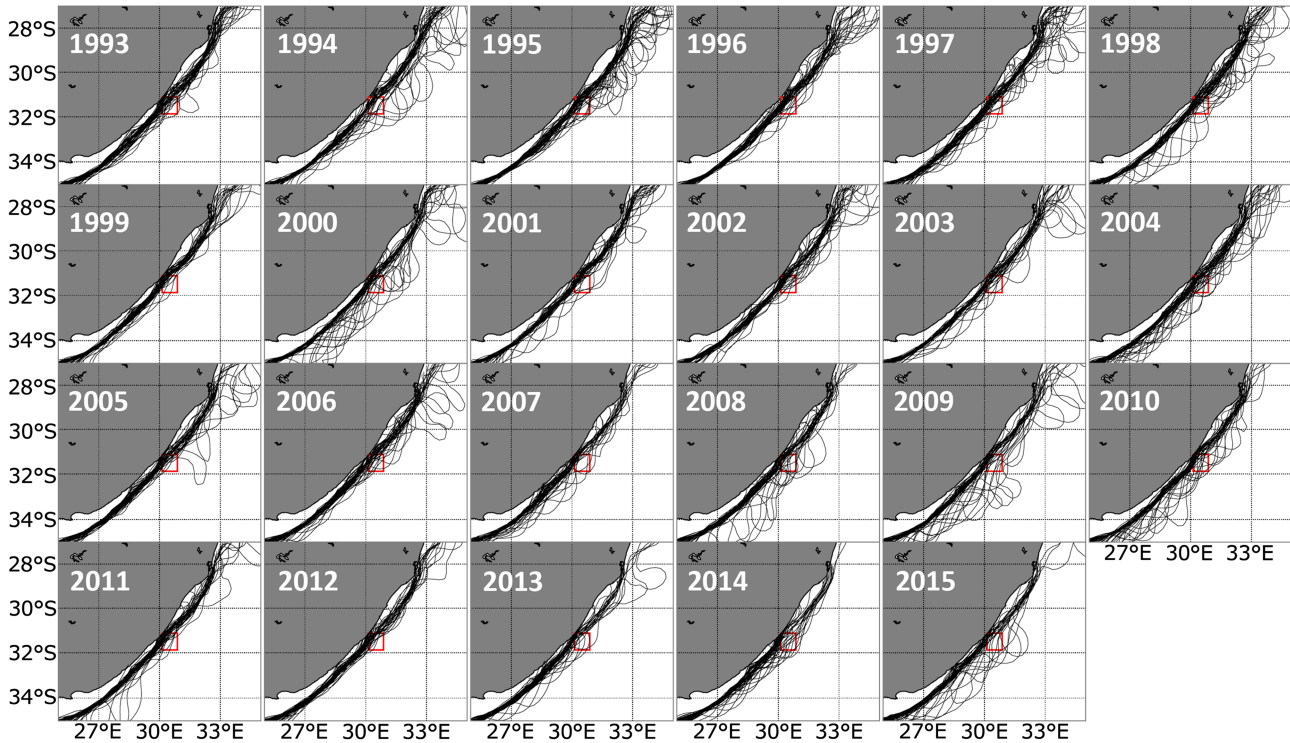
3. Model validation

We first check the general patterns of interannual stability of the Agulhas Current. Figure 1a shows weekly snapshots of 0.75 m ADT contours as a proxy for the core of the Agulhas Current. This method is inspired by the success in studies of the Kuroshio Extension region (Qiu & Chen, 2005). The Agulhas Current is stable in several years (1993, 1999, 2002, 2005, and 2012), while it appears to meander to the south of the Natal Bight ($\sim 31^\circ\text{S}$) in some other years (1998, 2000, 2004, 2008, 2009, 2010, 2013, and 2015). This implies the possible existence of interannual variations in the Natal Pulse. Note that since the current is relatively weak to the north of the Natal Bight ($\sim 28^\circ\text{S}$), disturbances of contours in the area indicate the approach of cyclonic eddies. Meanders in the OFES are larger than those in the AVISO (Figure 1b). In some years (1994, 1995, 2000, 2001, 2002, 2003, 2007, 2008, and 2010), deflections associated with cyclonic eddies (meanders) can be seen in the north (south) of the Natal Bight, while large deflections of contours are seen along the whole coast in other years (1997, 1998, 2005, 2012, and 2013; Figure 1b). Although this might be partly due to the underestimation of eddy dissipations (e.g. Braby et al., 2016), the trigger process of the Natal Pulse is relatively well reproduced in the OFES, which will be discussed in Sections 4.1 and 4.2. Notice that the interannual variations in the stability of the Agulhas Current are relatively well captured in the OFES. For example, the current is stable (unstable) in 1993, 2002, and 2006 (1994, 2003, and 2007) (Figure 1b).

To determine the Natal Pulse events, we define the Natal Pulse index (NPI) as area-averaged ADT within the red box ($30.125\text{-}30.875^\circ\text{E}$, $31.875\text{-}31.125^\circ\text{S}$) shown in Figure 1. Since the Natal Pulse is characterized by a negative coastal SLA, a negative peak is defined as a Natal Pulse event if the amplitude of this peak exceeds -2 standard deviations (Figures 2a, b). This definition enables us to identify 41 events from 1993 to 2015 in the AVISO data and 45 events from 1993 to 2013 in the OFES output. The number of events in this study is relatively fewer than in previous studies. For example, 1.8 per year in AVISO is found in this study, while about 2 per year at Port Edward (Figure 5d in Rouault & Penven, 2011). This is because we introduced a relatively high criterion, i.e. a negative peak beyond -2 standard deviations of SSH time series, to remove small-amplitude events. We note that the results are robust even if we change the size of the box to $0.5^\circ \times 0.5^\circ$ or $1.0^\circ \times 1.0^\circ$, while larger or smaller boxes do not capture cyclonic SLAs associated with the Natal Pulse. Since the size of Natal Pulse is around 100-150 km (Elipot & Beal, 2015), boxes smaller than $0.5^\circ \times 0.5^\circ$ cannot capture adequately the whole SLAs associated with a Natal Pulse. Also, boxes larger than $1.0^\circ \times 1.0^\circ$ may be contaminated by SLAs not related to the Natal Pulse. Since this study focuses on the relationship between incoming eddies and Natal Pulses, the box is set in the upstream compared to previous studies (e.g. Elipot & Beal, 2015). If we define the NPI in the downstream ($27.875\text{-}28.625^\circ\text{E}$, $33.875\text{-}33.125^\circ\text{S}$; similar to Elipot & Beal, 2015), the correlation of these time series is 0.60 and the number of the Natal Pulse in each year is qualitatively similar. Thus, our definition captures the characteristics of the Natal Pulse defined in previous studies well and the onset of the Natal Pulses associated with mesoscale eddies better.

Figure 3 shows the interannual variations in eddy kinetic energy (EKE) in the MC, south of Madagascar, and north and south of the Natal Bight, and the annual occurrence of the Natal Pulse. The occurrence of the Natal Pulse shows large interannual variations as described by the previous study (Elipot & Beal, 2015). Although some of the observed and simulated peaks are different (Figure 3a), variations in the OFES output show similar amplitude and frequency as those in the AVISO data. Also, the simulated mean and variance of EKE in each year resemble those in the AVISO (Figures 3b-e). Although the OFES does not exactly

(a) AVISO



(b) OFES

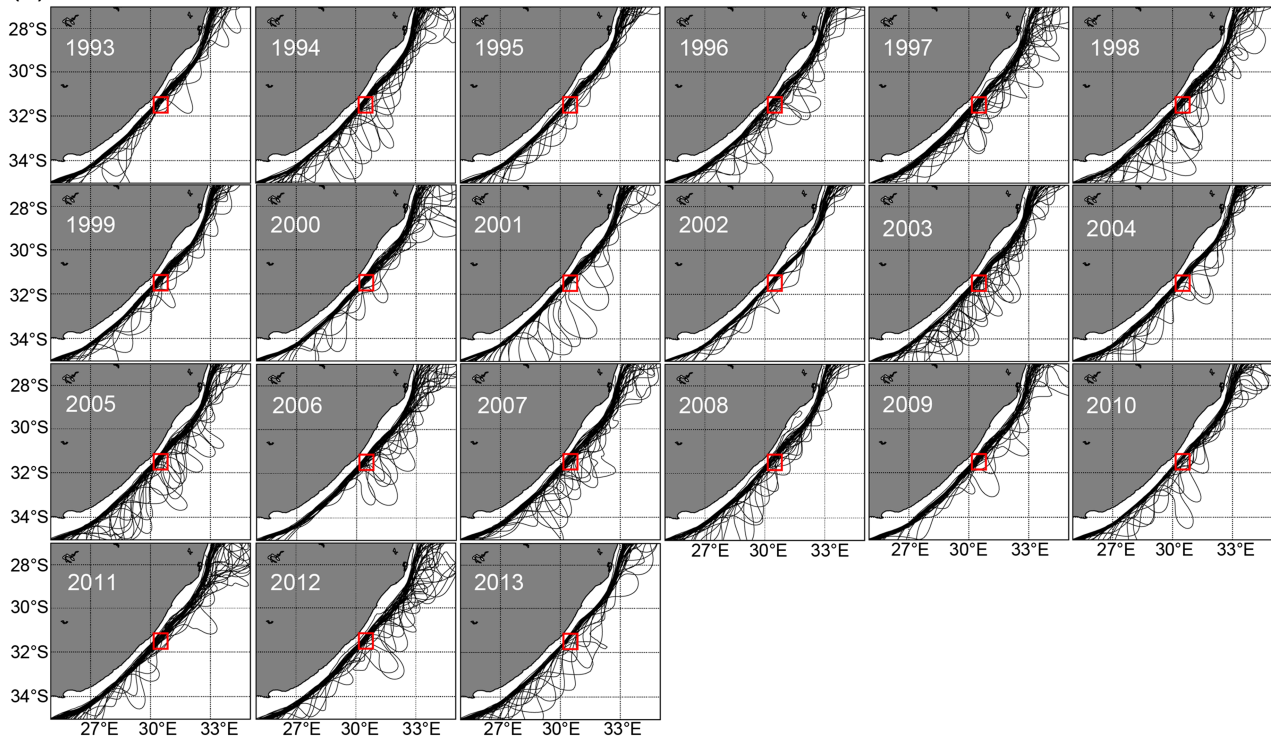


Figure 1. (a) Weekly 0.75 [m] contours of absolute dynamic topography (ADT) in each year from the AVISO dataset. (b) As in (a), but for 0.35[m] contours of sea surface height (SSH) from the OFES output. The 0.75 and 0.35 [m] contours are selected because both contours are close to the observed and simulated core of the Agulhas Current, respectively. Note that the reference values for ADT and SSH contours are different in (a) and (b) because their definitions are different. Only the longest contours in this domain are shown. The Natal Pulse index (NPI) is calculated within the red box (30.125-30.875°E, 31.875-31.125°S) in each panel. The red boxes represent the same area as the black boxes in Figures 4 and 5.

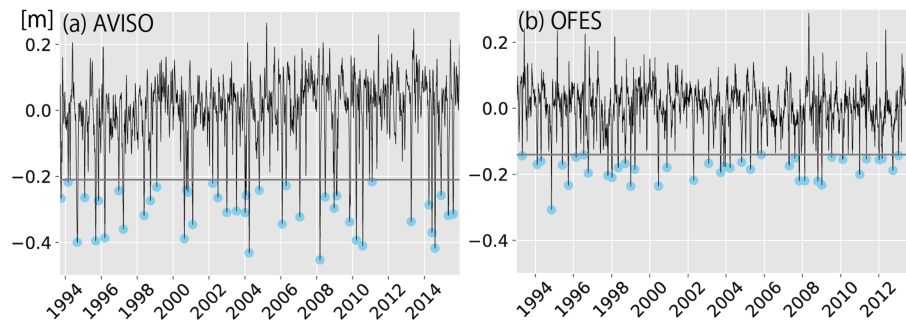


Figure 2. Time series of the NPI in (a) AVISO and (b) OFES. Monthly climatology is removed. The gray line represents -2 standard deviations, and all minima below this line are defined as the Natal Pulse events and indicated by blue markers.

reproduce each Natal Pulse event, it simulates the interannual variations of the Natal Pulse to some extent. The ability of the OFES will be further discussed in Section 4.1.

4. Sources of the Natal Pulse

Although incoming eddies as a trigger of the Natal Pulse have been suggested in previous studies (Braby et al., 2016; de Ruijter et al., 1999; Schouten et al., 2002; Tsugawa & Hasumi, 2010), their relative importance to the other mechanisms needs to be discussed. Regarding the interannual variations of the Natal Pulse, we examine whether the trigger of the Natal Pulse can be approximated by incoming anticyclonic eddies, and we find the sources of the Natal Pulse based on eddy-tracking results.

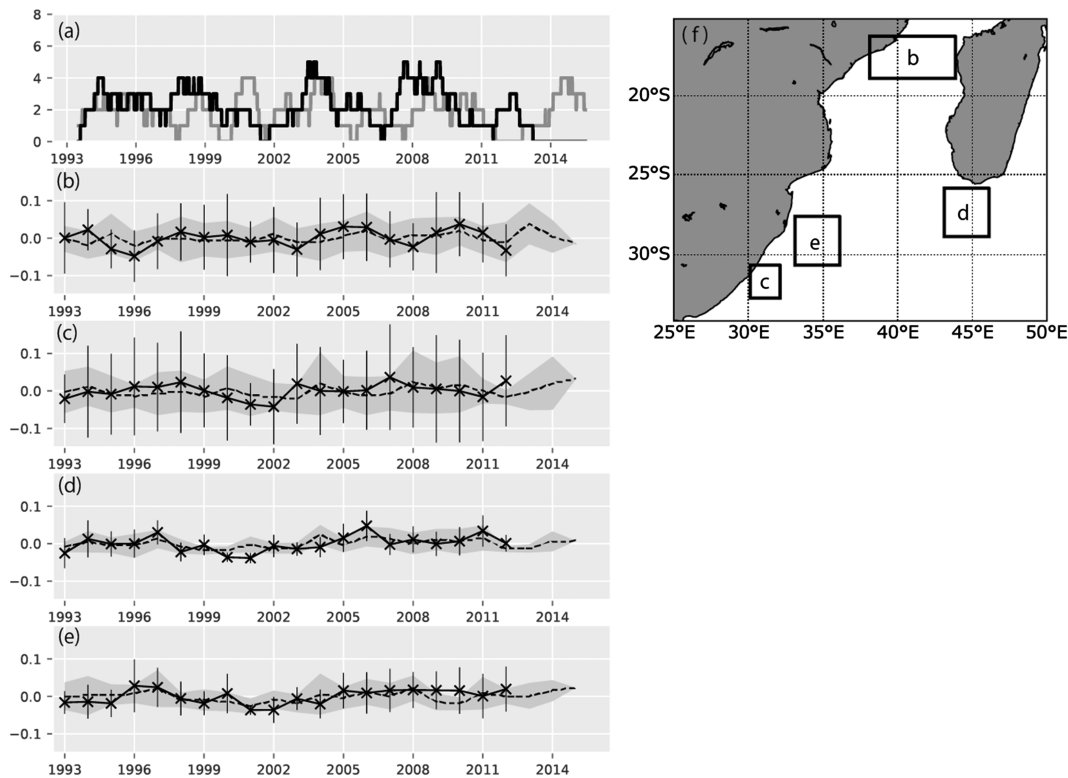


Figure 3. (a) Annual occurrence of the Natal Pulse with a 1-year running window. Gray (Black) colors signify the AVISO (OFES) results. Area averaged interannual variations of eddy kinetic energy (EKE) [m^2/s^2] in the boxes shown in (f), i.e. (b) MC (38.125–43.875°E, 18.875–16.125°S), (c) south of the Natal Bight (30.125–32.125°E, 32.625–30.625°S), (d) south of Madagascar (43.125–46.125°E, 28.875–25.875°S), and (e) north of the Natal Bight (33.125–36.125°E, 30.625–27.625°S). In (b)–(c), dashed (solid) lines show annually averaged EKE and gray shades (black bars) indicate ± 1 standard deviation of each year in the AVISO (OFES).

4.1. Role of eddy on the trigger of the Natal Pulse

To examine the triggering mechanism, a lag-composite analysis with a statistical test is conducted. Lag-composites of ADT indicate that cyclonic anomalies develop after the arrival of an anticyclonic eddy from the upstream (Figure 4). Statistically significant anticyclonic anomalies can be traced back for 40 days toward the upstream to about 27°S, but these signals become relatively weak further upstream. This may be because the anticyclonic signals arriving at the north of the Natal Bight come from several areas; the sources of anticyclonic eddies will be discussed in more detail in section 4.3. We note that this result is robust to slight changes in the box sizes and locations. Although there exist differences in the negative peaks between the AVISO and OFES results shown in Figures 2a, b, and 3a, the similarities in their lag-composites (Figure 4) indicate that the OFES output can be valuable for exploring the general characteristics of generation dynamics as well as interannual variability of the Natal Pulse occurrences.

We have also checked each event and examined whether anticyclonic or cyclonic eddies are detected around the Natal Bight (gray dashed rectangle in Figure 5) during the event using the eddy detection results. Although cyclonic eddies seem to approach south of the Natal Bight and connect to the Natal Pulse in few events (less than 10%) (Figure 5b), anticyclonic eddies are detected in the majority of events (about 80%) (Figure 5a) and trigger the Natal Pulse. Other events are hard to be classified from the SLA data. We note that positive SSH anomalies, which are deformed from a perfect circle and are therefore not defined as anticyclonic eddies, can be seen in most of the events. Therefore, the number of anticyclonic (cyclonic and the other) events may increase (decrease) if deformed positive SLA are detected more accurately. This result supports the idea that anticyclonic eddies are triggers of the many Natal Pulse events defined in this study.

4.2. Trigger of the Natal Pulse

In previous studies, the generation mechanism of the Natal Pulse was examined by calculating barotropic and baroclinic conversion rates (e.g. Elipot & Beal, 2015; Tsugawa & Hasumi, 2010). Here, a complete EKE budget during the Natal Pulse events are computed with the OFES output, and composite analyses are conducted with a statistical test, focusing on the role of anticyclonic eddies. In many studies, it was assumed *a priori* that barotropic and baroclinic conversions contribute instantaneously to changes in EKE, but other non-local terms, such as advection, work done by pressure, and dissipations, can also contribute to the time derivative of EKE with phase delays (Chen et al., 2014, 2016; Harrison & Robinson, 1978).

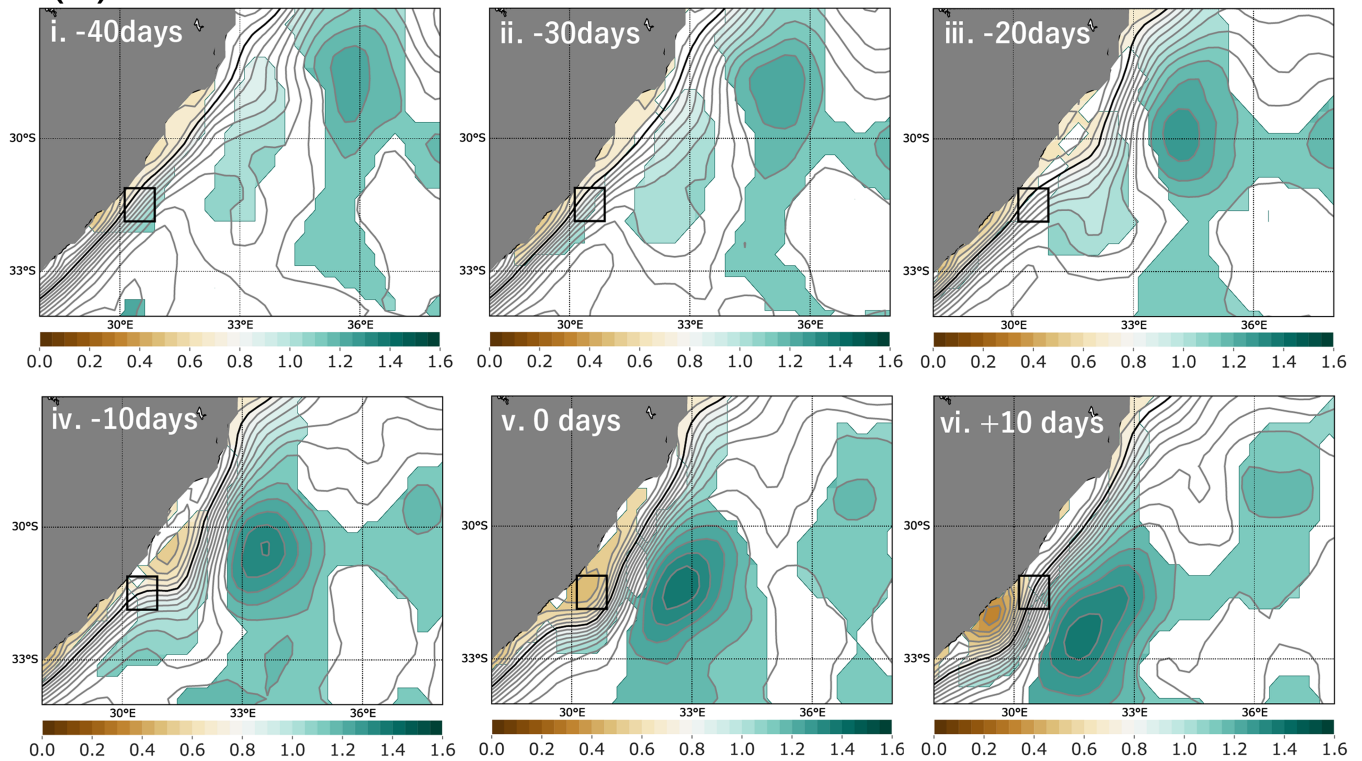
Following Chen et al. (2016), the time derivative of EKE ($=0.5\rho_0(u'^2+v'^2)$) is expressed as

$$\frac{\partial}{\partial t} EKE = \underbrace{\frac{\partial}{\partial x_i} (u_i EKE)}_{ADV} - \underbrace{\rho_0 u'_i u'_j \frac{\partial}{\partial x_j} \bar{u}_i}_{BT1} + \underbrace{\rho_0 u'_i \frac{\partial}{\partial x_j} \bar{u}_i u'_j}_{BT2} - \underbrace{\frac{\partial}{\partial x_i} (u'_i p')}_{Pressure} - \underbrace{g w' \rho'}_{BC} + \rho_0 u'_i D'_i \quad (2)$$

Here, $i = 1$ and 2 denote zonal and meridional directions, respectively; $j = 1, 2,$ and 3 denote zonal, meridional, and vertical directions, respectively; u_i is velocity, ρ_0 is the reference density ($=1025 \text{ kg m}^{-3}$), p is pressure, w is vertical velocity, and g is the gravitational acceleration. D'_i means a combination of vertical viscosity and horizontal biharmonic viscosity associated with u'_i . Also, an overbar is defined as the monthly mean climatology plus 1-year running mean field and is referred to as the "mean". A deviation from the mean field is represented by a prime and is referred to as "anomaly". We attempt to divide the variations in the Agulhas Current into the high frequency (shorter than sub-seasonal) and low frequency (longer than around 1-year). This definition allows us to examine whether the Natal Pulse is affected by the interannual (or longer time scale) variations in the Agulhas Current or not. Although this definition does not remove explicitly the instances of the Natal Pulse as in previous studies (e.g. Krug et al., 2014), the 1-year running mean is long enough to exclude the Natal Pulse instances.

On the right-hand side of Eq. (2), the first term represents advection (ADV), and the second and third terms represent momentum fluxes associated with the mean horizontal shear (BT1) and the mean of horizontal Reynolds stresses (BT2), respectively. The fourth term indicates work done by pressure (Pressure), and the fifth term represents buoyancy flux (BC). BT1 and BT2 are associated with the barotropic conversion, while BC is related to the baroclinic conversion.

(a) AVISO



(b) OFES

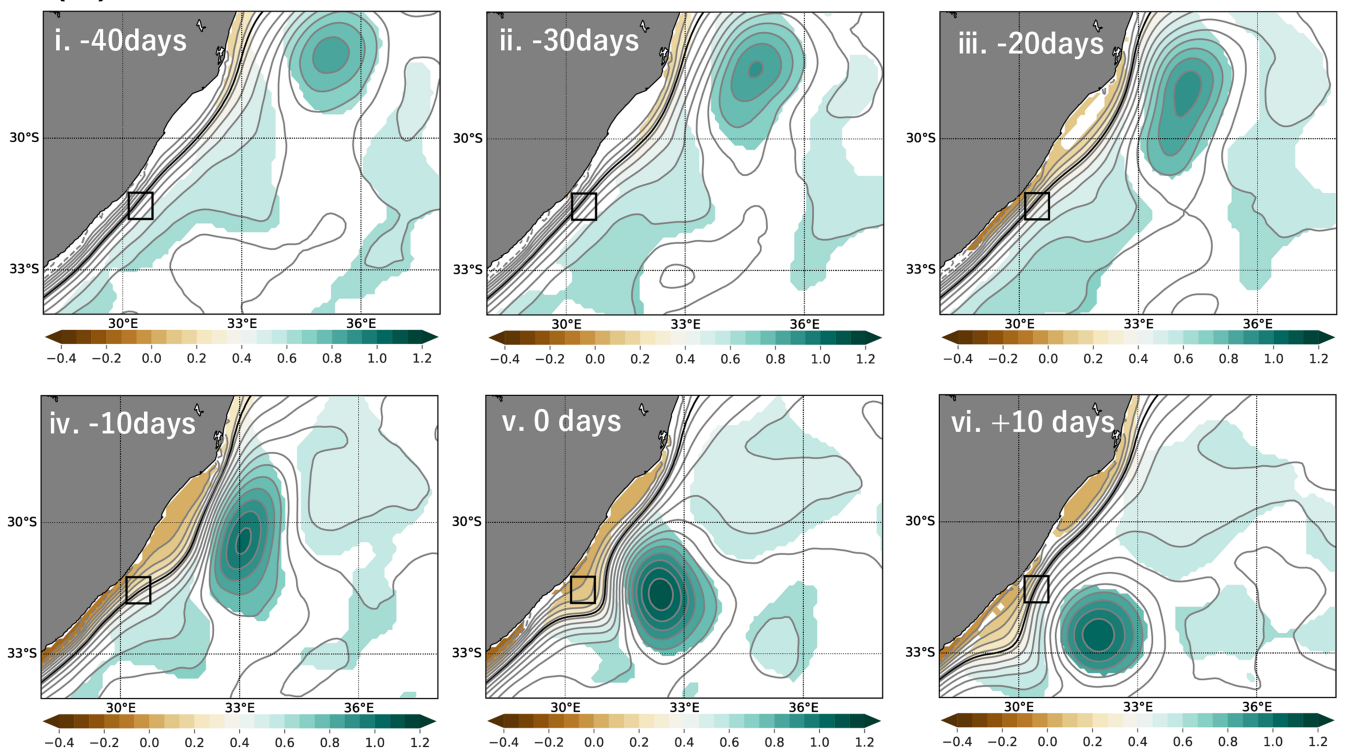


Figure 4. (a) Lag composites of ADT [m] from 40 days before to 10 days after the peak of the NPI in the AVISO dataset. (b) As in (a), but for SSH [m] in the OFES. Sea level anomalies (SLAs) above the 90% confidence level by a two-tailed t-test are shaded. The thick contour represents the 0.75 (0.35) m ADT (SSH) contour in the AVISO (OFES) and is used here as a proxy for the core of the Agulhas Current.

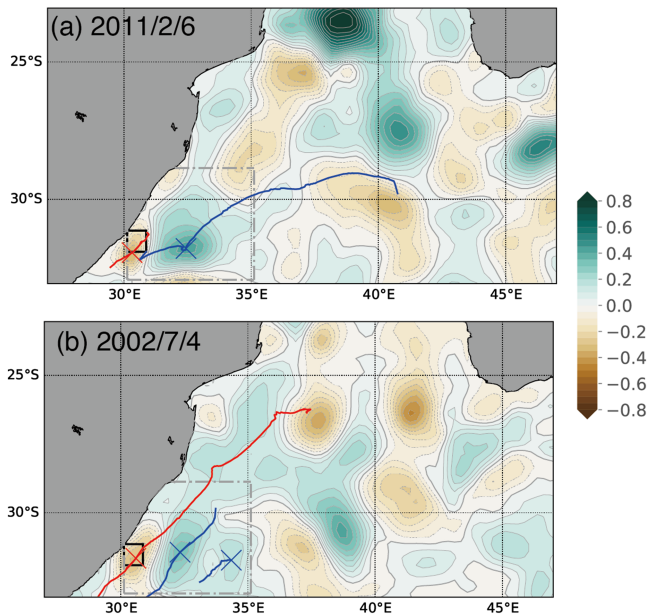


Figure 5. Examples of the Natal Pulse triggered by (a) an anticyclonic eddy and (b) a cyclonic eddy in AVISO. Shades show the snapshot of SLA [m], blue (red) lines and crosses indicate the track and center of anticyclonic (cyclonic) eddy from the eddy-tracking method. Gray dot dashed rectangles show the area in which the existence of the eddies is tested.

We calculate all terms except for the last term in Eq. (2) because the viscosity terms, which are important for forming the bottom current over the continental shelf slope (Holloway, 1992), are not available in the OFES output. Figure 6 shows lag composites of EKE anomalies and each term in Eq. (2) at 21, 12, and 3 days before the peak of the Natal Pulse. At Day -21, an anticyclonic eddy approaches the northern part of the Natal Bight (Figure 6a), where the mean southwestward Agulhas Current exists. As a result, interaction between horizontal shear and the eddy occurs and the barotropic conversion starts to increase while other terms remain small (Figures 6b-f). At Day -12, the barotropic conversion is further enhanced along the western flank of the incoming anticyclonic eddy (around 32°E in Figure 6c). Since these EKE anomalies are also advected by horizontal velocities of the eddy and/or the Agulhas Current itself, the maximum of the time derivative of EKE is located slightly to the downstream of the barotropic conversion maximum (Figures 6a, b, c). At Day -3, cyclonic anomalies in the coastal region are now well developed. The advection and barotropic conversion terms contribute to the maintenance of the meander (Figures 6b, c). In the southern (northern) part of the coastal cyclonic eddy, EKE increases (decreases) due to the advection and barotropic conversion, supporting the southwestward propagation of this meander. We note that the other terms are small over the entire period.

In light of the results of Lutjeharms et al. (2001) and the EKE budget analysis shown in Figure 6, bottom velocity anomalies during the Natal Pulse are expected to be small. Vertical structures of velocity anomalies suggest that there is no apparent interaction with the bottom topography and the velocity structure is quite barotropic in OFES (figure not shown).

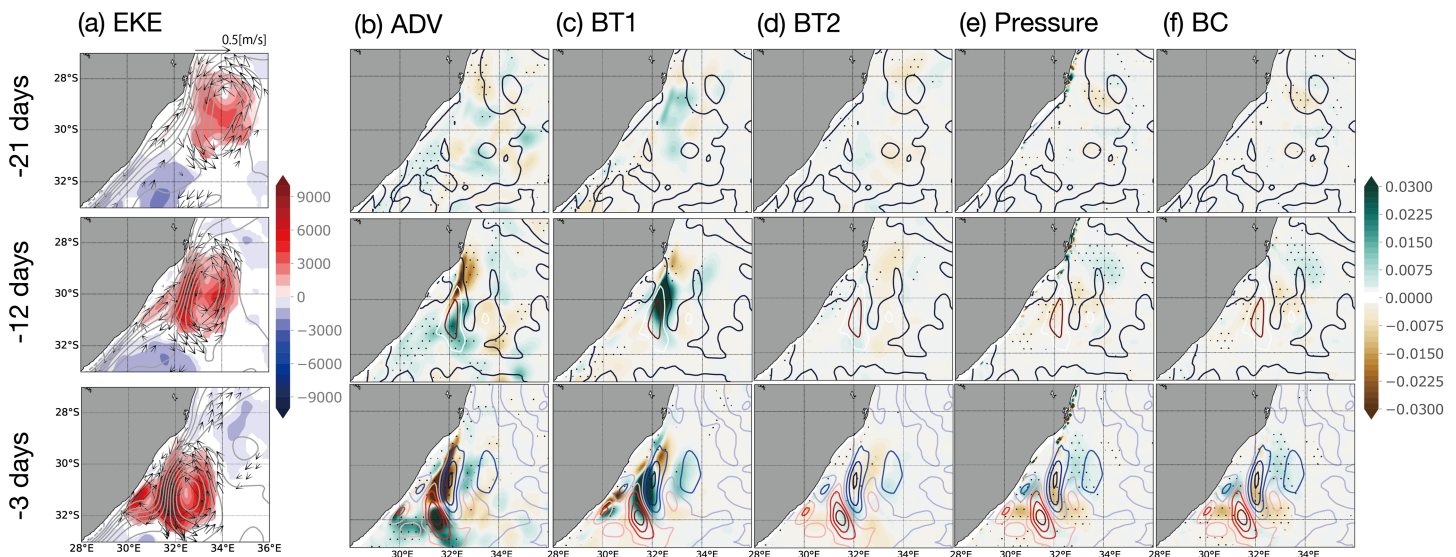


Figure 6. Lag composites of (a) EKE anomaly [kg/s^2] (color), ADT (contour), and velocity at 100 m depth (vector) 21 (top), 12 (middle), and 3 (bottom) days before the peak of the Natal Pulse in the OFES. (b)-(f) Same as (a), but for each term of Eq. (2). Color shows (b) advection (ADV), momentum flux associated with (c) mean horizontal shear (BT1) and (d) mean of horizontal Reynolds stress (BT2), (e) work done by pressure (Pressure), and (f) buoyancy flux (BC). Contours in (b)-(f) indicate the time derivative of EKE. Contour intervals are 0.006 kg/s^3 with the red (blue) contours denoting positive (negative) values. Shading and vectors in (a) and dots in (b)-(f) show anomalies above the 90% confidence level by a two-tailed t-test. Values in (b)-(f) are vertically integrated above 1300 m depth (below this depth, anomalies are relatively small) and their units are [kg/s^3].

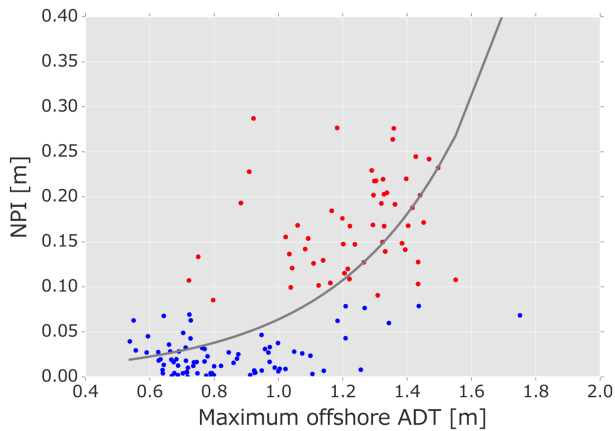


Figure 7. Scatter diagram between amplitude of all minima of the NPI and the maximum in concurrent ADT off the Natal Bight (31–34°E, 32–29°S). Red dots represent Natal Pulse events defined in this study, and blue dots indicate weak minima of the NPI which are not classified into the Natal Pulse events. The solid curve indicates a regression.

Also, we have further examined the dependency of the Natal Pulse on the strength of incoming anticyclonic eddies. The relationship between minima of the NPI and maximum ADTs off the Natal Bight shows that the strength of the negative anomalies along the coast corresponds well with the strength of the maximum offshore ADT (Figure 7). Note that some large positive SLAs do not seem to trigger the Natal Pulse (e.g. the blue dot at the right end of Figure 7) because anticyclonic eddies are away from the coast after interactions with the current in the north of the Natal Bight.

We also calculated the EKE budget for weak negative peaks which do not meet the below -2 standard deviation criterion of the NPI (blue dots in Figure 7). It is found that weak anticyclonic eddies do not trigger significant cyclonic anomalies along the coast (Figure 8). At Day -21, an anticyclonic eddy approaches the northern part of the Natal Bight (Figure 8a), as in Figure 6. However, interaction between horizontal shear and the eddy is relatively weak and the barotropic conversion starts to increase while other terms remain small (Figures 8b–f) at Day -12. At Day -3, cyclonic anomalies in the coastal region are not well developed, and the advection and barotropic conversion terms do not contribute to the development of the meander (Figures 8b, c).

Since there is no relationship between the Natal Pulse and the volume transport of the Agulhas Current (Leber & Beal, 2014) and no role of other eddy characteristics is found (e.g. radius, life, and nonlinearity), our result indicates that a strong incoming anticyclonic eddy is one of the necessary conditions for triggering of the Natal Pulse. We note that this relation can also be seen in the Kuroshio path changes (Endoh & Hibiya, 2001), and thus this result may suggest a general relationship between meanders of western boundary currents and anticyclonic eddies.

4.3. Sources of the anticyclonic eddies

Since anticyclonic eddies propagating along the coast trigger the Natal Pulse, we investigate the sources of these eddies using the eddy-tracking results. For this purpose, we count the number of anticyclonic eddies which pass north of the Natal Bight (33–36°E, 27–30°S) and classify these eddies based on their origins: (1) MC (north of 25°S), (2) SEMC (east of 40°E), and (3) local (others). Since the first two are the main sources

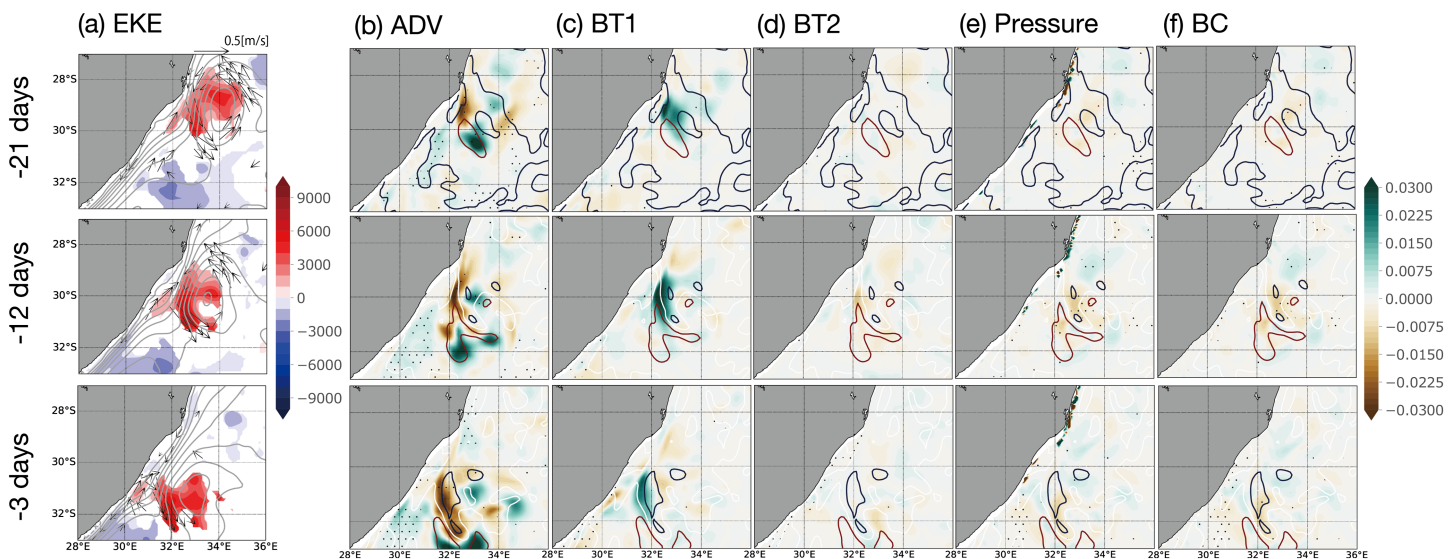


Figure 8. As in Figure 6, but for weak negative peaks of the NPI which are not defined as the Natal Pulse.

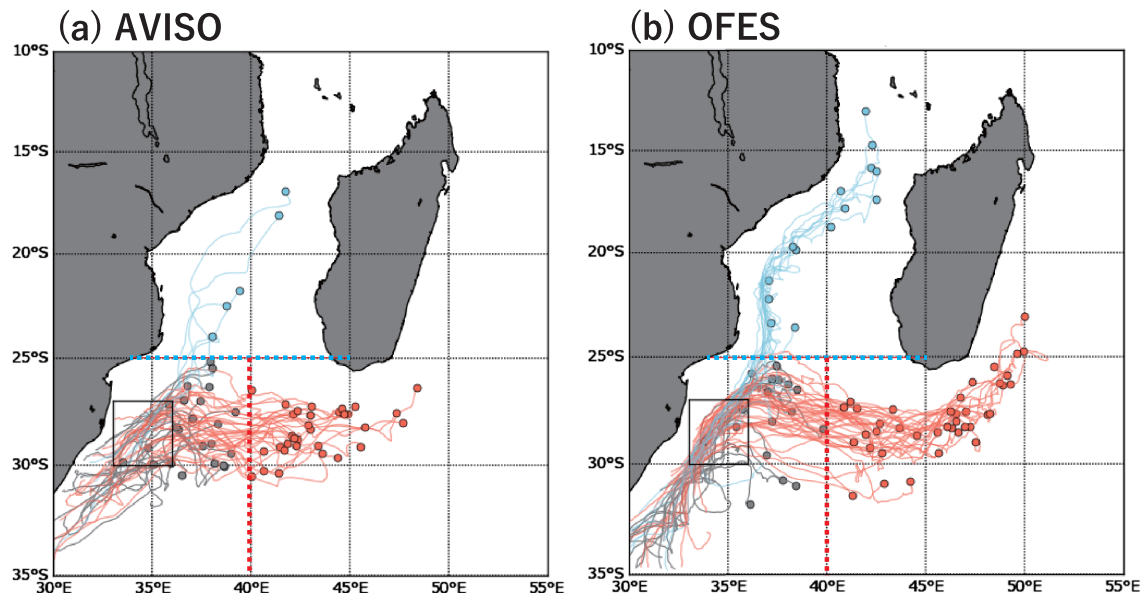


Figure 9. Eddy tracks which pass the black box (33–36°E, 30–27°S) in (a) AVISO and (b) OFES. Dots represent the origin of each anticyclonic eddy. Eddies originating from the Southeast Madagascar Current (SEMC) (east of 40°E shown by the red dotted line), Mozambique Channel (MC) (north of 25°S shown by the blue dotted line), and other regions (gray) are indicated.

of mesoscale eddies in the southwestern Indian Ocean (de Ruijter et al., 2004; Halo, Penven, et al., 2014; Halo, Backeberg, et al., 2014; Schouten et al., 2002, 2003), we mainly focus on eddies from these two regions.

The distribution of eddy birth points is similar to a previous study (Figure 1b of Braby et al., 2016), and the majority of the observed and simulated eddies passing through north of the Natal Bight is from the SEMC (Figure 9). It is found that in the AVISO (OFES), 33 (40) eddies originate from the SEMC, while 5 (15) eddies are from the MC (Table 1). Compared to the OFES, eddies in the AVISO tend to dissipate slower upon approaching the Agulhas Current (Figure 9), which is a common limitation of ocean models in this region (e.g. Backeberg et al., 2014). However, since the triggering processes of the Natal Pulse in the OFES are well reproduced (Figure 4), the use of the OFES output is justified. Note that a larger number of anticyclonic eddies than the Natal Pulses means that some anticyclonic eddies do not trigger the Natal Pulse. This is due to the strength of the eddy mentioned in Section 4.2. If the amplitude of the anticyclonic eddy were small, the eddy-induced coastal negative SSH anomaly does not develop enough to be defined as the Natal Pulse in this study (Figures 7, 8). Notice that the total number of eddies in the AVISO data tends to be smaller than in the OFES because of interruptions of eddy-tracking in the AVISO (Appendix A) that can hamper the eddy detection algorithm from tracking eddies for long distance.

5. Interannual variability of the Natal Pulse

In this section, interannual variability of the Natal Pulse will be discussed since the interannual variations in the Natal Pulse may be a key to understand interannual variability of the Agulhas Current and Agulhas Leakage. Note that no significant seasonal variations are found in the occurrence of the Natal Pulse events, as reported by Krug and Tournadre (2012).

5.1. Relative importance of anticyclonic eddies from different regions

Since anticyclonic eddies from upstream of the Natal Bight play a critical role in the generation of the Natal Pulse as mentioned in section 4, we investigate the contributions of these eddies using a Bayesian Poisson regression model (e.g. Gelman et al., 2013). If the probability ($p(y_i | \lambda_i)$) of the Natal Pulse occurrence in year- i (y_i) follows the Poisson distribution,

Table 1
Number (Percentage) of anticyclonic eddies which pass the north of the Natal Bight (the black box in Figure 9).

	SEMC	MC	Local
AVISO	33 (54%)	5 (8%)	23 (38%)
OFES	40 (56%)	15 (21%)	17 (24%)

Table 2

Posterior distribution of parameter values from the regression model (Eq. (4)) in the OFES. 2.5% and 97.5% indicate bottom and upper bounds of the estimated distribution of each parameter for the 95% credible interval.

	β_1	$\beta_2(\text{SEMC})$	$\beta_3(\text{MC})$	$\beta_4(\text{Local})$
2.5%	-0.72	0.046	-0.74	-0.23
Mean	0.19	0.29	-0.29	0.19
97.5%	1.1	0.53	0.17	0.63

$$p(y_i|\lambda_i) = \frac{\lambda_i^{y_i} \exp(-\lambda_i)}{y_i!}, \quad (3)$$

where λ_i is the average number of the Natal Pulse in year- i and is assumed as below:

$$\log(\lambda_i) = \beta_1 + \beta_2 x_{\text{SEMC},i} + \beta_3 x_{\text{MC},i} + \beta_4 x_{\text{Local},i} \quad (4)$$

Here, $x_{\text{SEMC},i}$, $x_{\text{MC},i}$, and $x_{\text{Local},i}$ are the number of anticyclonic eddies in year- i from the SEMC, MC, and Local regions, respectively. The logarithmic function on the left-hand side of Eq. (4) is a link function, which is often used for a Poisson regression model (e.g. McCullagh & Nelder, 1989). To fit the model, the noninformative prior distributions for each parameter are set, and posterior distributions are computed by the Markov Chain Monte Carlo method using PyMC3 (Salvatier et al., 2016). This statistical model expresses that the mean of the probability distribution of the Natal Pulse occurrence in a given year is explained by the arrival of anticyclonic eddies from three different source regions. We note that interannual autocorrelations of the Natal Pulse and eddies are small, and thus it is assumed that each variable in each year is independent of the others.

The values of β_j ($j = 1, 2, 3, 4$) are summarized in Table 2, and the time series of the annual occurrence of the Natal Pulse obtained from the OFES output and the regression model are shown in Figure 10. The regression model (λ_i) well reproduces the interannual variations of the Natal Pulse events, and the contribution from the SEMC eddies is relatively large. Although the number of samples is relatively small, β_2 is larger than 0 ($0.046 < \beta_2 < 0.53$) at the 95% credible interval (Table 2). Thus, the contribution of eddies from the SEMC is significant. If β_2 is set to the average value ($=0.29$) and $x_{\text{SEMC},i}$ is set to 1, λ_i is 1.3. This means that the regression model estimates 1.3 Natal Pulse from one SEMC eddy on average. In fact, a simple correlation coefficient of the Natal Pulse with the SEMC eddy is 0.46, while that with the MC and Local eddies are 0.31 and 0.13, respectively. These results indicate that anticyclonic eddies from the SEMC region have the strongest control over the interannual variations of the Natal Pulse, and eddies from the MC play a secondary role. This may be simply because the number of SEMC eddies is larger than that from other regions.

We also apply this method (Figure 10c) and an advanced version of this method, i.e. hierarchical Poisson regression modeling (Gelman et al., 2013), to the result in the AVISO. Although a relatively weak relationship between eddies and the Natal Pulse can be seen (Figure 10c), effects of the SEMC eddy are not significant (Table 3). Rather, the contribution of the local eddy is relatively large (Table 3). We note that this may be due to difficulties in tracking eddies in the AVISO (Appendix A) or a small sample number of years. Once the eddy-tracking results in the AVISO are corrected, the relationship between eddies and the Natal Pulse may be explained by the number of anticyclonic eddies as in the OFES (Appendix A). Improving the eddy-tracking algorithm and further accumulation of the observational data are needed in future studies. Hereafter, we focus on the tracking results of the OFES.

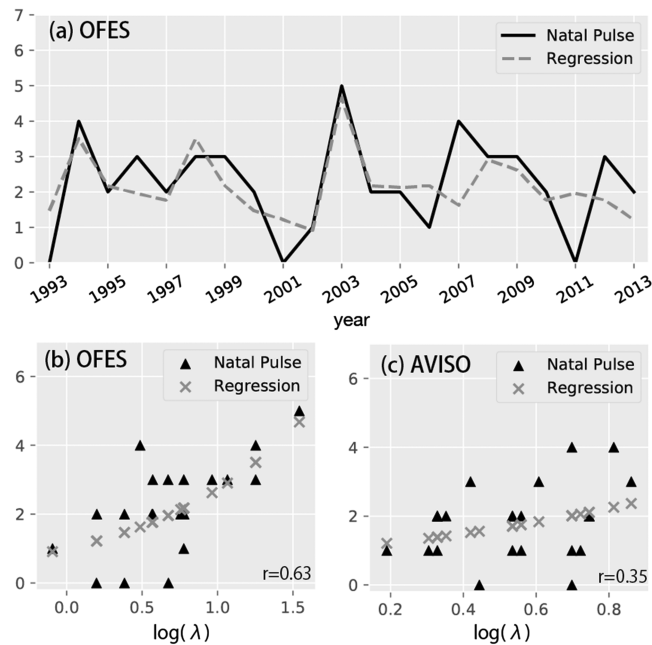


Figure 10. (a) Interannual variations of the Natal Pulse (black) and the time series reproduced by the Poisson regression model (gray) of Eq. (4) in the OFES. The vertical axis indicates the number of the Natal Pulse in each year. (b) As in (a), but for λ of Eq. (4) as the horizontal axis. (c) As in (b), but for the AVISO. Correlation coefficients between the Natal Pulse and the regression are shown in the lower right of (b) and (c).

5.2. Variability of anticyclonic eddies in the SEMC

Since the eddy-tracking result reveals that the anticyclonic eddies that trigger Natal Pulses mostly originate off the southeastern and southern coast of Madagascar (Figure 9), we compare the energy conversion rates and the number of anticyclonic eddies generated within the black dashed box in Figure 11a. Although eddies are also generated along the western coast of Madagascar, these eddies do not reach the north of the Natal Bight (Figure 9b) and thus they are excluded from the present analysis.

Interannual variations of the energy conversion rates and the birth number of eddies are shown in Figure 11b. It is found that the barotropic

Table 3
As in Table 2, but for the AVISO.

	β_1	$\beta_2(\text{SEMC})$	$\beta_3(\text{MC})$	$\beta_4(\text{Local})$
2.5%	-0.11	-0.46	-0.36	-0.13
Mean	0.53	-0.12	0.023	0.14
97.5%	1.1	0.22	0.40	0.41

conversion dominates over the baroclinic conversion during the whole period and that the annual birth number of anticyclonic eddies corresponds relatively well with the barotropic conversion ($r=0.50$). The barotropic conversion is large along the southeastern coast of Madagascar due to the horizontal shear of the SEMC (de Ruijter et al., 2004; Halo, Penven, et al., 2014), and the baroclinic conversion is small to the east of Madagascar. Hence, the interannual variations of the SEMC may explain those of the SEMC eddies that, in turn, influence the interannual variations of the Natal Pulse.

5.3. Connection between the wind stress field in the southern Indian Ocean and the Natal Pulse

Several studies have investigated the low-frequency ocean circulation and climate in the southern Indian Ocean associated with the El Niño/Southern Oscillation (ENSO) (e.g. Rao & Behera, 2005; Ridderinkhof et al., 2013; Yamagami & Tozuka, 2015; Zhuang et al., 2013), Indian Ocean Dipole (Palastanga et al., 2006), and Ningaloo Niño (Kataoka et al., 2014). Since wind stress curl variability to the south of 10° is explained by the ENSO (Rao & Behera, 2005), here we assume wind stress curl variability in the southern Indian Ocean represents ENSO variability. Since the interannual variations of the SEMC are explained by wind stress field variations through the linear Rossby-wave response (Yamagami & Tozuka, 2015), we investigate the connection between Natal Pulse and large-scale wind stress curl in the southern Indian Ocean. We construct a regression model similar to Eq. (4) using wind stress curl anomalies in the interior region with 12 months lag as below,

$$\log(\lambda_i) = \beta_1 + \beta_2 x_{wind,i-12} \quad (5)$$

We set the lag as 12 months because the lag correlation between wind stress and the Natal Pulse is maximum ($r=0.52$) at this lag (Figure 12b). This time lag is reasonable for the propagation of Rossby waves and eddies from the interior region to the Natal Bight (Yamagami & Tozuka, 2015). Since the regression model shows a significant effect (Figure 12c) and reproduces the number of the Natal Pulse relatively well, the interannual variations of the Natal Pulse are linked with the ENSO via atmospheric teleconnections to the southern Indian Ocean. We note that a not-so-high correlation between the Natal Pulse and wind stress field does not necessarily indicate a weak connection between the Natal Pulse and the ENSO. This may be partly because the propagation speed of Rossby waves and/or eddies are not constant and partly because not all anticyclonic eddies cause a Natal Pulse.

6. Discussion and Summary

In this study, we have investigated the sources of the Natal Pulse trigger using the AVISO ADT dataset and the OFES output. Composite analysis and eddy-tracking results reveal the role of anticyclonic eddies in triggering the Natal Pulse. We have also conducted an EKE budget analysis with a statistical test and found that the barotropic conversion due to the mean shear of the Agulhas Current and the advection of EKE dominate the EKE growth significantly in a large number of Natal Pulse events. Thus, as suggested by previous studies (e.g. Tsugawa & Hasumi, 2010), incoming anticyclonic eddies play an important role in triggering of the Natal Pulse, but this study has shown this by the composite analysis with a statistical test and a complete EKE budget analysis for the first time. The relationship between amplitudes of the coastal cyclonic anomaly and the maximum ADT off the Natal Bight suggests that the amplitude of the anticyclonic eddies, which mainly come from the SEMC, is also important for the growth of the Natal Pulse.

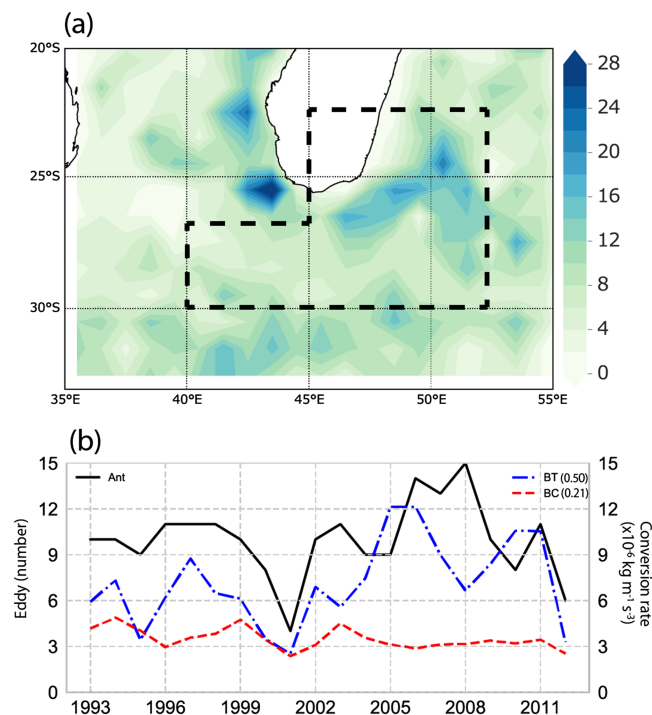


Figure 11. (a) Number of anticyclonic eddies generated from 1993 to 2013 in the OFES within $1^\circ \times 1^\circ$ box. The coordinates of black dashed box are the combination of $40^\circ\text{--}45^\circ\text{E}$, $30^\circ\text{--}26.5^\circ\text{S}$ and $45^\circ\text{--}52^\circ\text{E}$, $30^\circ\text{--}20^\circ\text{S}$. (b) Interannual anomalies of the barotropic (blue) and baroclinic (red) conversion rate [10^{-6} kg/m^3] averaged within the black dashed box in (a). The black solid line indicates the number of anticyclonic eddies detected in the black dashed box in (a). Correlations between conversion rates and the number of eddies are shown in the upper right corner.

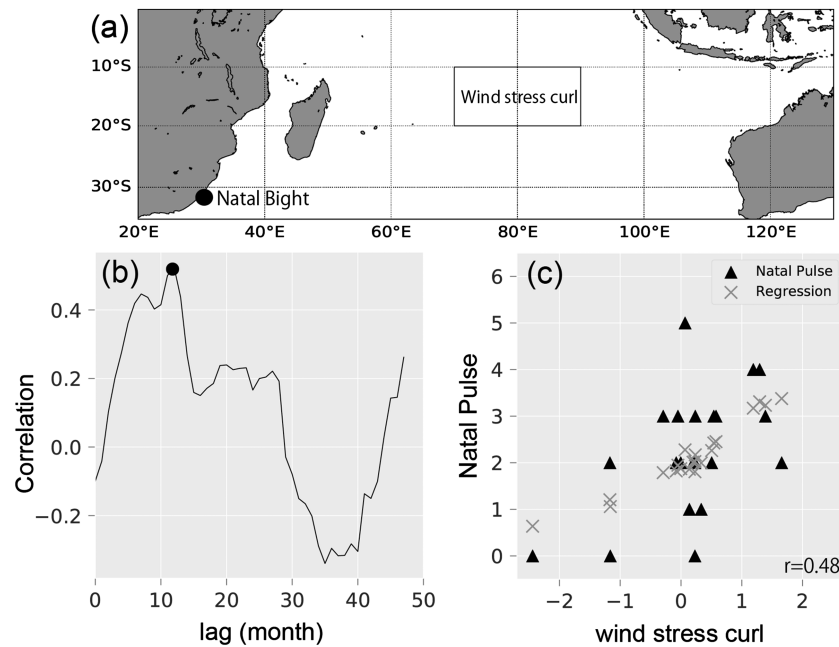


Figure 12. (a) Schematic diagram of the area where wind stress curl anomalies are averaged (box; 70°-90°E, 20°-10°S) and the Natal Bight (dot). (b) Lag correlation between wind stress curl anomalies averaged over the box in (a) and the number of Natal Pulses in the OFES. The dot indicates the maximum lag correlation. (c) Interannual variations of the Natal Pulse (black) and the time series reproduced by the regression model (gray) in the OEFS with a 12-month lag (Eq. (5)). The vertical axis indicates the number of Natal Pulses in each year, while the horizontal axis shows normalized wind stress curl anomalies. Their correlation coefficient is shown in the lower right corner.

The mechanism of the interannual variations of the Natal Pulse is also discussed in this study. The occurrence of the Natal Pulse shows interannual variations in both AVISO and OFES. A simple statistical model reveals the importance of anticyclonic eddies originating from the SEMC. An energy conversion analysis off the southern coast of Madagascar shows the importance of the barotropic conversion. Also, it is shown that the interannual variations of the energy transfer from the SEMC itself play a critical role in the interannual variations of the Natal Pulse. A relationship between wind stress curl anomalies in the southern Indian Ocean and the Natal Pulse is also revealed by a statistical model. This result suggests that the interannual variations of the Natal Pulse are linked with the ENSO-modulated wind stress forcing over the interior South Indian Ocean.

This study is originally motivated by possible impacts of interannual variations of the trade winds to the interannual variations in the Agulhas Current and Agulhas Leakage. Although Ridderinkhof et al. (2013) showed the connection between EKE in the southwestern Indian Ocean and ENSO using the correlation analysis, the framework that the climate variation phenomenon is a driver of the mesoscale activity in the southwestern Indian Ocean has not been examined dynamically. Also, Elipot and Beal (2015) reported that most ring shedding events seem to occur independently, and thus suggested other local or remote mechanisms are candidates for the ring shedding and Agulhas leakage variability. Therefore, investigation of the linkage between climate variability in the southern Indian Ocean, the Natal Pulse, and Agulhas Leakage is the next step. One possible approach is multi-member ensemble simulations by a high-resolution OGCM. Nonaka et al. (2016) examined predictability of the Kuroshio Extension region and suggested that multi-member ensemble simulation is useful to understand the variability of the western boundary currents. Also, these simulations allow us to quantify contributions to the Agulhas Current system by forced components of the climate variabilities and by probabilistic components from local instability or eddy generation. Therefore, we believe that a multi-member ensemble simulation with different strength of the trade winds in the southern Indian Ocean associated with the ENSO will be valuable to understand how deterministic the Natal Pulse and Agulhas Leakage are.

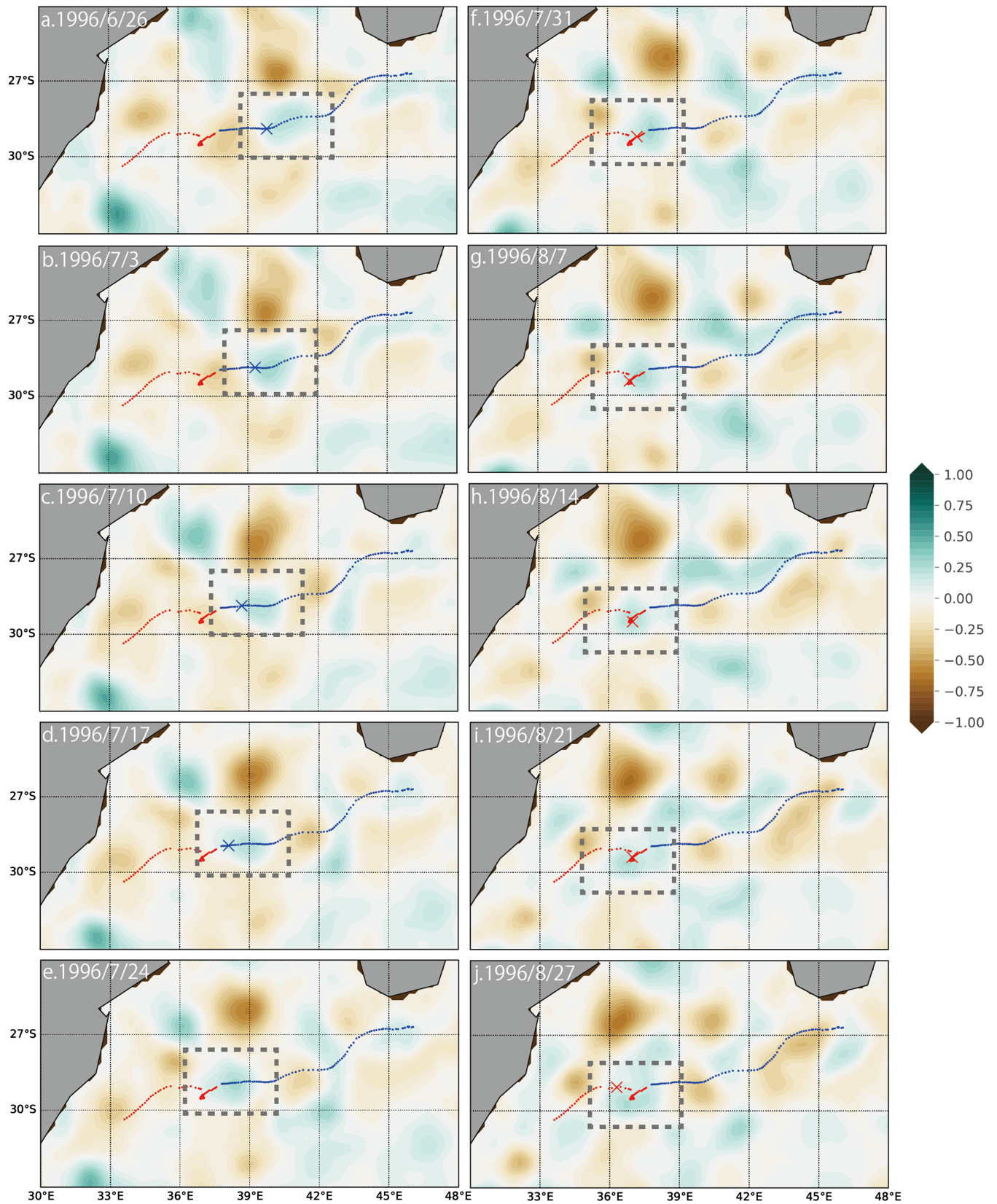


Figure A1. An example of the interruption of eddy-tracking in the AVISO. Weekly snapshots of centers (cross) and whole tracks (line) of anticyclonic eddies from July to August 1996 are shown in blue before and red after the interruption. Shading indicates SLA [m] in the AVISO.

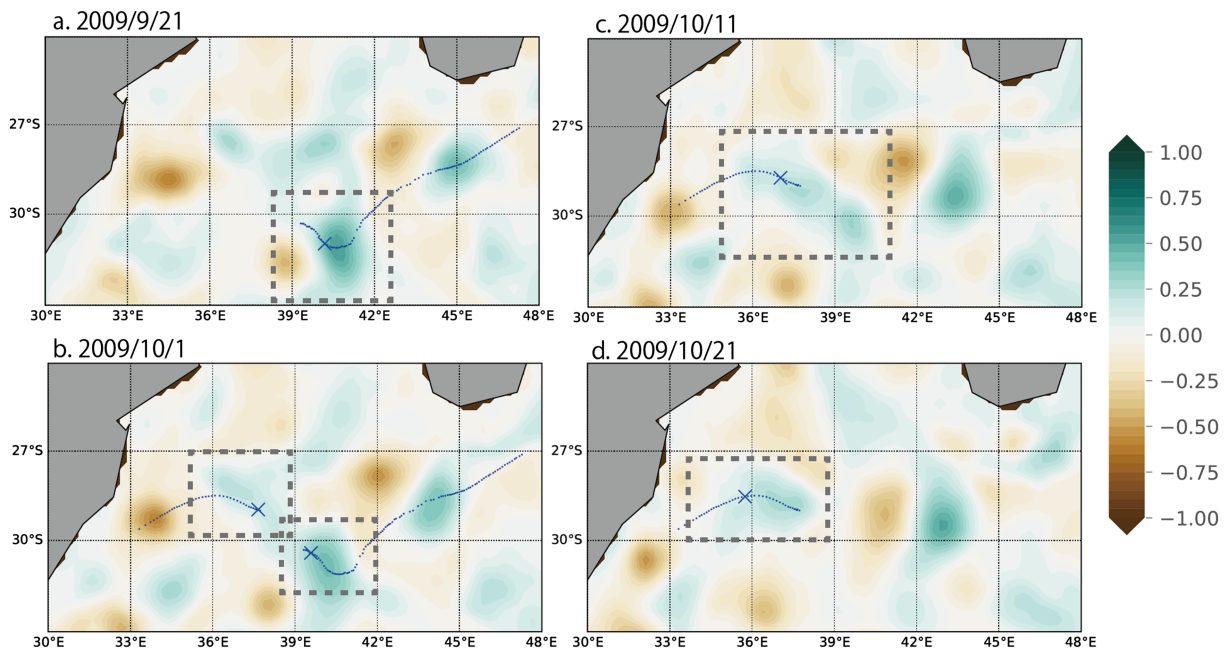


Figure A2. An example of the interruption of eddy-tracking in the AVISO due to the eddy-eddy interaction. Weekly snapshots of centers (cross) and whole tracks (line) of anticyclonic eddies from September to October 2009 are shown in blue. Shading indicates SLA [m] in the AVISO.

Modeling of the southwestern Indian Ocean is quite challenging. Although the MC is a pathway of low-frequency variability from the tropical southern Indian Ocean to the Agulhas Leakage (Putrasahan et al., 2016) and anticyclonic eddies from the MC play some role in the interannual variations of the Natal Pulse, no OGCM has succeeded in realistically simulating the frequency and variability of the circulation in the MC (van der Werf et al., 2010). Therefore, further effort is necessary for more realistic eddy-resolving simulations of the Natal Pulse and another mesoscale variability in the greater Agulhas system to improve the understanding and prediction of this key region in the global climate system.

Appendix A.: Eddy-tracking in AVISO

The differences in eddy-tracking results between AVISO and OFES are investigated in this appendix. First, statistics of eddy characteristics around the south of Madagascar are compared between AVISO and OFES, and it is found that eddy life in the AVISO is shorter than that in the OFES, while eddy amplitude, radius, energy, and nonlinearity are similar. This is partly due to the failure of the eddy-tracking in the AVISO (Figure A1). In AVISO, interruption of eddy-tracking during the propagation of an anticyclonic eddy from the south of Madagascar to the Natal Bight tends to occur more frequently than OFES. This leads to more local eddies in the AVISO (Table 1); the correlation between interannual variations of local eddies and SEMC eddies in the AVISO ($r = -0.57$) is larger than that in the OFES ($r = 0.25$).

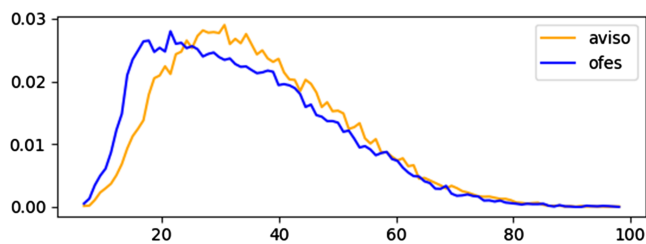


Figure A3. Shape errors probability distribution of anticyclonic eddies in south of Madagascar from eddy-tracking results using 100% shape test criterion. Blue (orange) line represents OFES (AVISO). The vertical axis indicates probability density, while the horizontal axis shows the shape error [%].

Examining snapshots of the SLA and eddy-tracking results reveals that mesoscale eddies in the AVISO are often distorted and jump to other eddies (Figure A2). It is found that these distortions and jumps disturb the eddy-tracking, which was reported by Braby et al. (2016). In Figure A2, after an anticyclonic eddy approaches another one, these eddies seem to interact with each other and merge into one anticyclonic eddy. Since the eddy-tracking scheme considers certain eddies as new eddies when the repositioning occurs due to the assimilation of the AVISO data into the model around the Agulhas Current (de Vos et al.,

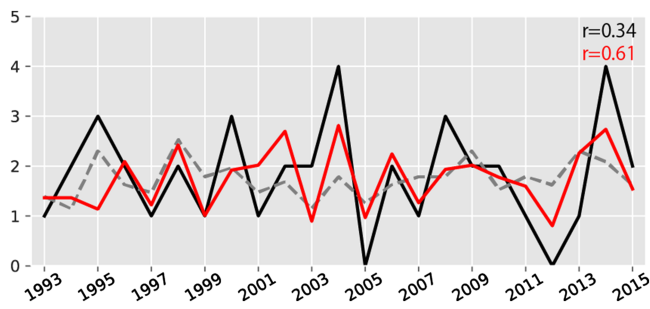


Figure A4. As in Figure 10a, but for the AVISO. Interannual variations of the Natal Pulse (black), the time series reproduced by the regression model from the eddy-tracking results without (gray dashed) and with (red) the correction. Correlation coefficients between the Natal Pulse and the regression models are shown in the upper right.

Acknowledgments

We would like to thank two anonymous reviewers and Bjorn Backeberg for their reviews and for providing helpful comments. The major part of this paper was from a Ph.D. thesis from the University of Tokyo. Y. Yamagami's thesis committee (Hiroyasu Hasumi, Toshiyuki Hibiya, Yukio Masumoto, and Hiroaki Miura) provided valuable comments and suggestions. We also thank Shuiming Chen for his helpful comments. The altimeter products were produced and distributed by AVISO (<http://www.aviso.altimetry.fr/duacs/>) and now by Copernicus Marine Environment Monitoring Service (<http://marine.copernicus.eu>). The OFES integrations were performed on the Earth Simulator under the support of the Japan Agency for Marine-Earth Science and Technology (JAMSTEC). The OFES data is provided by Asia-Pacific Data Research Center (<http://apdrc.soest.hawaii.edu>), which is a part of the International Pacific Research Center at the University of Hawaii at Manoa, funded in part by the National Oceanic and Atmospheric Administration (NOAA). py-eddy-tracker (Mason et al., 2014) is available under a GNU license (<http://imedeia.uib-csic.es/users/emason/py-eddy-tracker/>). Y. Yamagami is supported by MEXT through the Integrated Research Program for Advancing Climate Models, JSPS KAKENHI grant 15J08994, and Leading Graduate Course for Frontiers of Mathematical Sciences and Physics at the University of Tokyo.

2018), it is speculated that this is one of the errors inherent in the AVISO dataset.

Since changes of some criteria in the eddy-tracking algorithm are expected to improve the eddy-tracking results in the AVISO, sensitivities of the criteria are examined. The criteria are shape error, local maximum, and search area size in subsequent frames of the eddy-tracking (see Chelton et al., 2011). The results are not so sensitive to changes in the shape error (from 55%, 100%, and 120%) and the local maximum criteria (1, 2, and 10). Also, an increase of the search area size (from 1 to 3, 4, and 5 times) leads to more frequent occurrences of jumping from one track to another. For example, eddy-tracking using local maximum = 2 improves the tracking of the anticyclonic eddy shown in Figure A1. However, the results still show artifacts in many cases since the tracking stops when the eddy-eddy interaction (i.e. the split, merger, deformation, and rapid move of the center of eddies) seems to occur. In the OFES, shape

error of anticyclonic eddies is less than the AVISO (Figure A3), and the number of jumps between eddies seems to be smaller. This is a desirable condition for eddy-tracking to work.

To avoid the artificial terminations and births of eddies, eddy-tracking results in the AVISO are corrected in the following way, which is similar to Braby et al. (2016). First, after the termination of each track, eddies that are born within 14-day and 150 km-radius from the end point of the eddy are chosen for the candidates of the same eddy. This 14-day is selected because artificial ends and births of eddies seem to occur within two weeks. The 150 km-radius, which is used for the minimum search area in Chelton et al. (2011), is selected to avoid jumping to a different track. If more than one eddies are found, an eddy with minimum S (Eq. (1)) is selected as the same eddy. This method improves the eddy-tracking and the relationship between Natal Pulses and anticyclonic eddies in the AVISO (Figure A4) to some extent. The regression model without the correction fails to reproduce interannual variations of the Natal Pulse (Figure A4), but the regression with the correction explains the time series of the Natal Pulse as well as in the OFES (Figures A4 and 10a). This result implies that the relationship between eddies and the Natal Pulse in the AVISO is also explained by the number of anticyclonic eddies as in the OFES. Although this correction method improves the eddy-tracking results in the AVISO, there remains uncertainty in the criteria for the search area (i.e. 150 km) and periods (14 days). Further investigations are necessary to develop an objective method to improve the eddy-tracking algorithm, but this is beyond the scope of this paper. Thus, we have decided to focus on the tracking results from the OFES in this study.

References

- Backeberg, B. C., Counillon, F., Johannessen, J. A., & Pujol, M. I. (2014). Assimilating along-track SLA data using the EnOI in an eddy resolving model of the Agulhas system. *Ocean Dynamics*, *64*(8), 1121–1136. <https://doi.org/10.1007/s10236-014-0717-6>
- Beal, L. M., de Ruijter, W. P., Biastoch, A., Zahn, R., Cronin, M., & Hermes, J. (2011). On the role of the Agulhas system in ocean circulation and climate. *Nature*, *472*(7344), 429–436. <https://doi.org/10.1038/nature09983>
- Beal, L. M., & Elipot, S. (2016). Broadening not strengthening of the Agulhas Current since the early 1990s. *Nature*, *540*(7634), 570–573. <https://doi.org/10.1038/nature19853>
- Beal, L. M., Elipot, S., Houk, A., & Leber, G. M. (2015). Capturing the transport variability of a western boundary jet: Results from the Agulhas Current Time-Series experiment (ACT). *Journal of Physical Oceanography*, *45*(5), 1302–1324. <https://doi.org/10.1175/JPO-D-14-0119.1>
- Beron-Vera, F. J., Wang, Y., Olascoaga, M. J., Goni, G. J., & Haller, G. (2013). Objective Detection of Oceanic Eddies and the Agulhas Leakage. *Journal of Physical Oceanography*, *43*(7), 1426–1438. <https://doi.org/10.1175/JPO-D-12-0171.1>
- Biastoch, A., Böning, C. W., & Lutjeharms, J. R. E. (2008). Agulhas leakage dynamics affects decadal variability in Atlantic overturning circulation. *Nature*, *456*(7221), 489–492. <https://doi.org/10.1038/nature07426>
- Biastoch, A., Böning, C. W., Schwarzkopf, F. U., & Lutjeharms, J. R. E. (2009). Increase in Agulhas leakage due to poleward shift of Southern Hemisphere westerlies. *Nature*, *462*(7272), 495. <https://doi.org/10.1038/nature08519>
- Biastoch, A., Durgadoo, J. V., Morrison, A. K., van Sebille, E., Weijer, W., & Griffies, S. M. (2015). Atlantic multi-decadal oscillation covaries with Agulhas leakage. *Nature Communications*, *6*, 10082. <https://doi.org/10.1038/ncomms10082>
- Braby, L., Backeberg, B. C., Anson, I., Roberts, M. J., Krug, M., & Reason, C. J. C. (2016). Observed eddy dissipation in the Agulhas Current. *Geophysical Research Letters*, *43*, 8143–8150. <https://doi.org/10.1002/2016GL069480>
- Bryden, H. L., Beal, L. M., & Duncan, L. M. (2005). Structure and transport of the Agulhas current and its temporal variability. *Journal of Oceanography*, *61*(3), 479–492. <https://doi.org/10.1007/s10872-005-0057-8>
- Chelton, D. B., Schlax, M. G., & Samelson, R. M. (2011). Global observations of nonlinear mesoscale eddies. *Progress in Oceanography*, *91*(2), 167–216. <https://doi.org/10.1016/j.pocan.2011.01.002>

- Chelton, D. B., Schlax, M. G., Samelson, R. M., & de Szoeke, R. A. (2007). Global observations of large oceanic eddies. *Geophysical Research Letters*, *34*, L15606. <https://doi.org/10.1029/2007GL030812>
- Chen, R., Flierl, G. R., & Wunsch, C. (2014). A description of local and nonlocal eddy–mean flow interaction in a global eddy-permitting state estimate. *Journal of Physical Oceanography*, *44*(9), 2336–2352. <https://doi.org/10.1175/JPO-D-14-0009.1>
- Chen, R., Thompson, A. F., & Flierl, G. R. (2016). Time-dependent eddy-mean energy diagrams and their application to the ocean. *Journal of Physical Oceanography*, *46*(9), 2827–2850. <https://doi.org/10.1175/JPO-D-16-0012.1>
- de Ruijter, W. P. M., van Aken, H. M., Beier, E. J., Lutjeharms, J. R. E., Matano, R. P., & Schouten, M. W. (2004). Eddies and dipoles around South Madagascar: formation, pathways and large-scale impact. *Deep Sea Research Part I: Oceanographic Research Papers*, *51*(3), 383–400. <https://doi.org/10.1016/j.dsr.2003.10.011>
- de Ruijter, W. P. M., van Leeuwen, P. J., & Lutjeharms, J. R. E. (1999). Generation and evolution of Natal Pulses: solitary meanders in the Agulhas Current. *Journal of Physical Oceanography*, *29*(12), 3043–3055. [https://doi.org/10.1175/1520-0485\(1999\)029<3043:GAEONP>2.0.CO;2](https://doi.org/10.1175/1520-0485(1999)029<3043:GAEONP>2.0.CO;2)
- de Vos, M., Backeberg, B., & Counillon, F. (2018). Using an eddy-tracking algorithm to understand the impact of assimilating altimetry data on the eddy characteristics of the Agulhas system. *Ocean Dynamics*, *68*(9), 1071–1091. <https://doi.org/10.1007/s10236-018-1174-4>
- Durgadoo, J. V., Loveday, B. R., Reason, C. J. C., Penven, P., & Biastoch, A. (2013). Agulhas leakage predominantly responds to the Southern Hemisphere westerlies. *Journal of Physical Oceanography*, *43*(10), 2113–2131. <https://doi.org/10.1175/JPO-D-13-047.1>
- Durgadoo, J. V., Rühls, S., Biastoch, A., & Böning, C. W. B. (2017). Indian Ocean sources of Agulhas leakage. *Journal of Geophysical Research: Oceans*, *122*, 3481–3499. <https://doi.org/10.1002/2016JC012676>
- Elipot, S., & Beal, L. M. (2015). Characteristics, energetics, and origins of Agulhas Current meanders and their limited influence on ring shedding. *Journal of Physical Oceanography*, *45*(9), 2294–2314. <https://doi.org/10.1175/JPO-D-14-0254.1>
- Endoh, T., & Hibiya, T. (2001). Numerical simulation of the transient response of the Kuroshio leading to the large meander formation south of Japan. *Journal of Geophysical Research*, *106*(C11), 26833–26850. <https://doi.org/10.1029/2000JC000776>
- Gelman, A., Stern, H. S., Carlin, J. B., Dunson, D. B., Vehtari, A., & Rubin, D. B. (2013). *Bayesian Data Analysis*. Chapman and Hall/CRC. <https://doi.org/10.1201/b16018>
- Gill, A. E., & Schumann, E. H. (1979). Topographically Induced Changes in the Structure of an Inertial Coastal Jet: Application to the Agulhas Current. *Journal of Physical Oceanography*, *9*(5), 975–991. [https://doi.org/10.1175/1520-0485\(1979\)009<0975:TICITS>2.0.CO;2](https://doi.org/10.1175/1520-0485(1979)009<0975:TICITS>2.0.CO;2)
- Gründlingh, M. L. (1979). Observation of a large meander in the Agulhas Current. *Journal of Geophysical Research*, *84*(C7), 3776–3778. <https://doi.org/10.1029/JC084iC07p03776>
- Guastella, L. A., & Roberts, M. J. (2016). Dynamics and role of the Durban cyclonic eddy in the KwaZulu-Natal Bight ecosystem. *African Journal of Marine Science*, *38*, S23–S42. <https://doi.org/10.2989/1814232X.2016.1159982>
- Halo, I., Backeberg, B., Penven, P., Anson, I., Reason, C., & Ullgren, J. E. (2014). Eddy properties in the Mozambique Channel: A comparison between observations and two numerical ocean circulation models. *Deep Sea Research Part II: Topical Studies in Oceanography*, *100*, 38–53. <https://doi.org/10.1016/j.dsr2.2013.10.015>
- Halo, I., Penven, P., Backeberg, B., Anson, I., Shillington, F., & Roman, R. (2014). Mesoscale eddy variability in the southern extension of the East Madagascar Current: Seasonal cycle, energy conversion terms, and eddy mean properties. *Journal of Geophysical Research: Oceans*, *119*, 7324–7356. <https://doi.org/10.1002/2014JC009820>
- Harris, T. F. W., Legeckism, R., & Van Forest, D. (1978). Satellite infra-red images in the Agulhas Current System. *Deep Sea Research*, *25*, 543–548. [https://doi.org/10.1016/0146-6291\(78\)90642-2](https://doi.org/10.1016/0146-6291(78)90642-2)
- Harrison, D. E., & Robinson, A. R. (1978). Energy analysis of open regions of turbulent flows—Mean eddy energetics of a numerical ocean circulation experiment. *Dynamics of Atmospheres and Oceans*, *2*(2), 185–211. [https://doi.org/10.1016/0377-0265\(78\)90009-X](https://doi.org/10.1016/0377-0265(78)90009-X)
- Holloway, G. (1992). Representing topographic stress for large-scale ocean models. *Journal of Physical Oceanography*, *22*, 1033–1046. [https://doi.org/10.1175/1520-0485\(1992\)022<1033:RTSFLS>2.0.CO;2](https://doi.org/10.1175/1520-0485(1992)022<1033:RTSFLS>2.0.CO;2)
- Hughes, G. R., Luschi, P., Mencacci, R., & Papi, F. (1998). The 7000-km oceanic journey of a leatherback turtle tracked by satellite. *Journal of Experimental Marine Biology and Ecology*, *229*(2), 209–217. [https://doi.org/10.1016/S0022-0981\(98\)00052-5](https://doi.org/10.1016/S0022-0981(98)00052-5)
- Kalnay, E., Kanamitsu, M., Kistler, R., Collins, W., Deaven, D., Gandin, L., et al. (1996). The NCEP/NCAR 40-year reanalysis project. *Bulletin of the American Meteorological Society*, *77*(3), 437–471. [https://doi.org/10.1175/1520-0477\(1996\)077<0437:TNYRP>2.0.CO;2](https://doi.org/10.1175/1520-0477(1996)077<0437:TNYRP>2.0.CO;2)
- Kataoka, T., Tozuka, T., Behera, S., & Yamagata, T. (2014). On the Ningaloo Niño/Niña. *Climate Dynamics*, *43*(5–6), 1463–1482. <https://doi.org/10.1007/s00382-013-1961-z>
- Krug, M., & Tournadre, J. (2012). Satellite observations of an annual cycle in the Agulhas Current. *Geophysical Research Letters*, *39*, L15607. <https://doi.org/10.1029/2012GL052335>
- Krug, M., Tournadre, J., & Dufois, F. (2014). Interactions between the Agulhas Current and the eastern margin of the Agulhas Bank. *Continental Shelf Research*, *34*, 67–79. <https://doi.org/10.1016/j.csr.2014.02.020>
- Kurian, J., Colas, F., Capet, X., McWilliams, J. C., & Chelton, D. B. (2011). Eddy properties in the California Current System. *Journal of Geophysical Research*, *116*, C08027. <https://doi.org/10.1029/2010JC006895>
- Leber, G. M., & Beal, L. M. (2014). Evidence that Agulhas Current transport is maintained during a meander. *Journal of Geophysical Research: Oceans*, *119*, 3806–3817. <https://doi.org/10.1002/2014JC009802>
- Leber, G. M., Beal, L. M., & Elipot, S. (2016). Wind and current forcing combine to drive strong upwelling in the Agulhas Current. *Journal of Physical Oceanography*, *47*(1), 123–134. <https://doi.org/10.1175/JPO-D-16-0079.1>
- Loveday, B. R., Durgadoo, J. V., Reason, C. J. C., Biastoch, A., & Penven, P. (2014). Decoupling of the Agulhas Leakage from the Agulhas Current. *Journal of Physical Oceanography*, *44*(7), 1776–1797. <https://doi.org/10.1175/JPO-D-13-093.1>
- Lutjeharms, J. R. E. (1981). Features of the southern Agulhas Current circulation from satellite remote sensing. *South African Journal of Science*, *77*(5), 231–236.
- Lutjeharms, J. R. E. (2006). *The Agulhas Current*, (p. 329). New York: Springer.
- Lutjeharms, J. R. E., & Roberts, H. R. (1988). The Natal pulse: An extreme transient on the Agulhas Current. *Journal of Geophysical Research*, *93*(C1), 631–645. <https://doi.org/10.1029/JC093iC01p00631>
- Lutjeharms, J. R. E., van der Vaart, P. C. F., Rossby, T., & Bryden, H. L. (2001). Evidence that the Natal Pulse involves the Agulhas Current to its full depth. *Geophysical Research Letters*, *28*(18), 3449–3452. <https://doi.org/10.1029/2000GL012639>
- Mason, E., Pascual, A., & McWilliams, J. C. (2014). A new sea surface height-based code for oceanic mesoscale eddy tracking. *Journal of Atmospheric and Oceanic Technology*, *31*(5), 1181–1188. <https://doi.org/10.1175/JTECH-D-14-00019.1>
- Masumoto, Y., Sasaki, H., Kagimoto, T., Komori, N., Ishida, A., Sasai, Y., et al. (2004). A fifty-year eddy-resolving simulation of the world ocean: Preliminary outcomes of OFES (OGCM for the Earth Simulator). *Journal of Earth Simulator*, *1*, 35–56.
- McCullagh, P., & Nelder, J. A. (1989). *Generalized linear models*. Chapman and Hall/CRC.

- Nonaka, M., Sasai, Y., Sasaki, H., Taguchi, B., & Nakamura, H. (2016). How potentially predictable are midlatitude ocean currents? *Scientific Reports*, *6*(1), 20153. <https://doi.org/10.1038/srep20153>
- Palastanga, V., van Leeuwen, P. J., & de Ruijter, W. P. M. (2006). A link between low-frequency mesoscale eddy variability around Madagascar and the large-scale Indian Ocean variability. *Journal of Geophysical Research*, *111*, C09029. <https://doi.org/10.1029/2005JC003081>
- Penven, P., Echevin, V., Pasapera, J., Colas, F., & Tam, J. (2005). Average circulation, seasonal cycle, and mesoscale dynamics of the Peru Current System: A modeling approach. *Journal of Geophysical Research*, *110*, C10021. <https://doi.org/10.1029/2005JC002945>
- Penven, P., Lutjeharms, J. R. E., & Florenchie, P. (2006). Madagascar: A pacemaker for the Agulhas Current system? *Geophysical Research Letters*, *33*, L17609. <https://doi.org/10.1029/2006GL026854>
- Pujol, M. I., Faugère, Y., Taburet, G., Dupuy, S., Pelloquin, C., Ablain, M., & Picot, N. (2016). DUACS DT2014: the new multi-mission altimeter data set reprocessed over 20 years. *Ocean Science*, *12*(5), 1067–1090. <https://doi.org/10.5194/os-12-1067-2016>
- Putrasahan, D., Kirtman, B. P., & Beal, L. M. (2016). Modulation of SST interannual variability in the Agulhas leakage region associated with ENSO. *Journal of Climate*, *29*(19), 7089–7102. <https://doi.org/10.1175/JCLI-D-15-0172.1>
- Qiu, B., & Chen, S. (2005). Variability of the Kuroshio Extension jet, recirculation gyre, and mesoscale eddies on decadal time scales. *Journal of Physical Oceanography*, *35*(11), 2090–2103.
- Randall, R. M., Randall, B. M., & Baird, D. (1981). Speed of Movement of Jackass Penguins over Long Distances and their Possible Use of Ocean Currents. *South African Journal of Science*, *77*(9), 420–429.
- Rao, S. A., & Behera, S. K. (2005). Subsurface influence on SST in the tropical Indian Ocean: Structure and interannual variability. *Dynamics of Atmospheres and Oceans*, *39*(1-2), 103–135. <https://doi.org/10.1016/j.dynatmoce.2004.10.014>
- Ridderinkhof, W., Le Bars, D., Heydt, A. S., & Ruijter, W. P. M. (2013). Dipoles of the South East Madagascar Current. *Geophysical Research Letters*, *40*, 558–562. <https://doi.org/10.1002/grl.50157>
- Rouault, M. J., & Penven, P. (2011). New perspectives on Natal Pulses from satellite observations. *Journal of Geophysical Research*, *116*, C07013. <https://doi.org/10.1029/2010JC006866>
- Salvatier, J., Wiecki, T. V., & Fonnesbeck, C. (2016). Probabilistic programming in Python using PyMC3. *Peer Journal Computer Science*, *2*, e55. <https://doi.org/10.7717/peerj-cs.55>
- Schouten, M. W., de Ruijter, W. P. M., & van Leeuwen, P. J. (2002). Upstream control of Agulhas Ring shedding. *Journal of Geophysical Research*, *107*(C8), 3109. <https://doi.org/10.1029/2001JC000804>
- Schouten, M. W., de Ruijter, W. P. M., van Leeuwen, P. J., & Ridderinkhof, H. (2003). Eddies and variability in the Mozambique Channel. *Deep Sea Research Part II: Topical Studies in Oceanography*, *50*(12–13), 1987–2003. [https://doi.org/10.1016/S0967-0645\(03\)00042-0](https://doi.org/10.1016/S0967-0645(03)00042-0)
- Siedler, G., Rouault, M., Biastoch, A., Backeberg, B., Reason, C. J., & Lutjeharms, J. R. (2009). Modes of the southern extension of the East Madagascar Current. *Journal of Geophysical Research*, *114*, C01005. <https://doi.org/10.1029/2008JC004921>
- Souza, J. M. A. C. D., de Boyer Montégut, C., & Le Traon, P. Y. (2011). Comparison between three implementations of automatic identification algorithms for the quantification and characterization of mesoscale eddies in the South Atlantic Ocean. *Ocean Science*, *7*(3), 317–334. <https://doi.org/10.5194/os-7-317-2011>
- Tsugawa, M., & Hasumi, H. (2010). Generation and growth mechanism of the Natal Pulse. *Journal of Physical Oceanography*, *40*(7), 1597–1612. <https://doi.org/10.1175/2010JPO4347.1>
- van der Werf, P. M., van Leeuwen, P. J., Ridderinkhof, H., & de Ruijter, W. P. M. (2010). Comparison between observations and models of the Mozambique Channel transport: Seasonal cycle and eddy frequencies. *Journal of Geophysical Research*, *115*, C02002. <https://doi.org/10.1029/2009JC005633>
- van Leeuwen, P. J., de Ruijter, W. P. M., & Lutjeharms, J. R. E. (2000). Natal pulses and the formation of Agulhas rings. *Journal of Geophysical Research*, *105*(C3), 6425–6436. <https://doi.org/10.1029/1999JC900196>
- Yamagami, Y., & Tozuka, T. (2015). Interannual variability of South Equatorial Current bifurcation and western boundary currents along the Madagascar coast. *Journal of Geophysical Research: Oceans*, *120*, 8551–8570. <https://doi.org/10.1002/2015JC011069>
- Zhuang, W., Feng, M., Du, Y., Schiller, A., & Wang, D. (2013). Low-frequency sea level variability in the southern Indian Ocean and its impacts on the oceanic meridional transports. *Journal of Geophysical Research: Oceans*, *118*, 1302–1315. <https://doi.org/10.1002/jgrc.20129>